X-RAY LASER PHYSICS

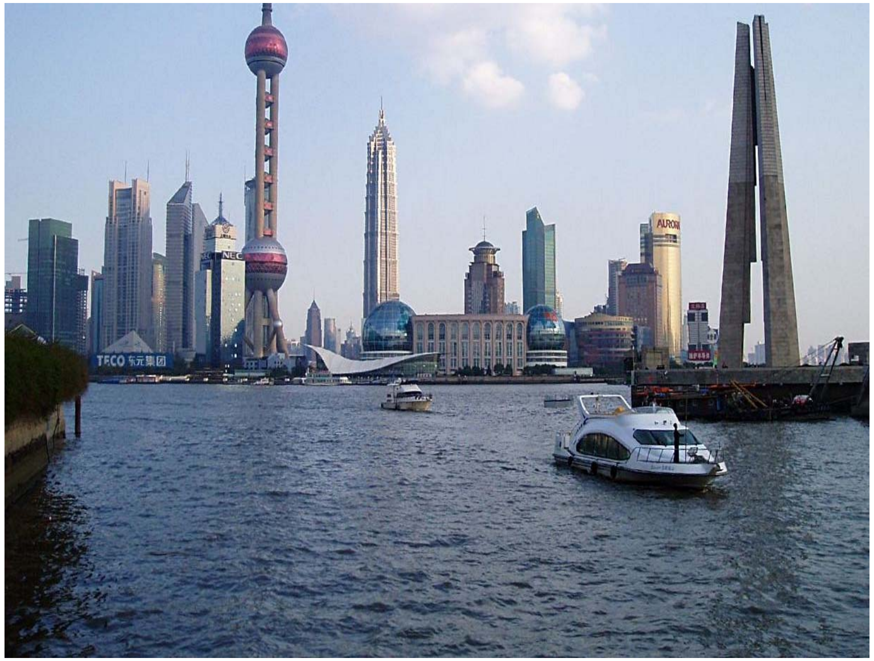

Shanghai Jiao Tong University, Shanghai, China

Charles K. Rhodes
Jiao Tong University
Shanghai, China
October 27-31 2008

X-Ray Amplification

Two Key Innovations

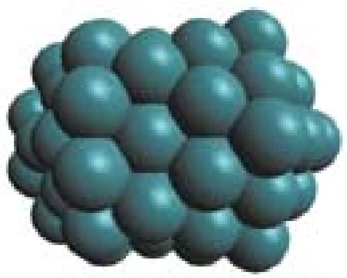

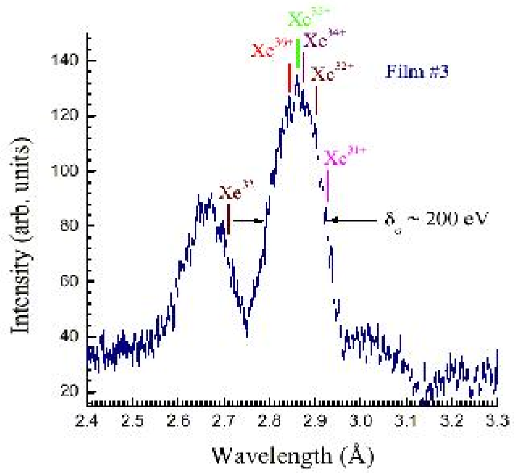

- **Channeled Propagation**
  → Spatial Organization

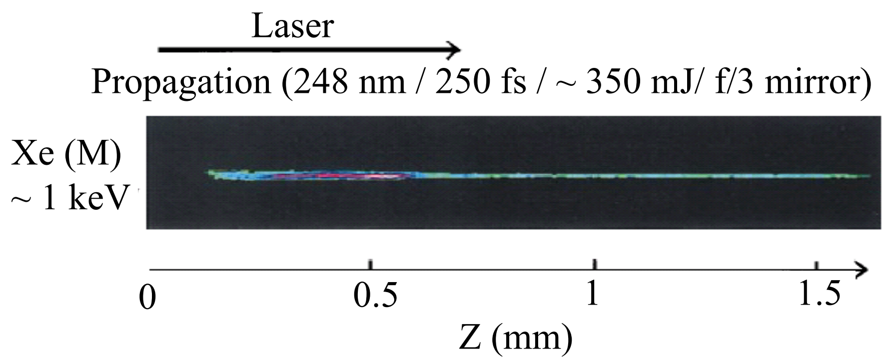

Historical Paper

In their seminal paper "Infrared and Optical Masers" published in *The Physical Review* in 1958, Arthur L. Schawlow and Charles H. Townes concluded with a section in which they discussed the high-frequency limits of amplification [1]. They wrote "unless some radically new approach is found," the x-ray zone is out of reach. Furthermore, the last sentence of the same article stated "…continuous tuning over larger ranges of frequency will require materials with very special properties." In relation to the work described below, the former requirement is satisfied by the development of a new concept that involves radiation dominated energy flow under conditions for which the phase space of the interaction is precisely controlled while the latter is met by the use of hollow atoms.

[1] Townes and Schawlow, Phys. Rev. **112**, 1940 (1958)

Key Concept → Controlled Power Compression

Why X-Rays?
Power Density Scaling

→ TRANSITION TO X-RAY REGIME

- Basic Parameter (wavelength) Changed by > 10^3

$$1 \text{ eV (IR)} \xrightarrow[\sim 4500]{\lambda^{-1}} 4.5 \text{ keV (X-Ray)}$$

- Radiative Rates Scale Like ~ λ^{-3}

$(4500)^3 \sim 9 \times 10^{10}$

- Area Scales ~ λ^{-2} (Channeling)

$(4500)^2 \sim 2 \times 10^7$

- Combined Power Density Scaling

→ λ^{-6} → $(4500)^6 \sim 8 \times 10^{21}$

- HUGE FAVORABLE POWER COMPRESSION SCALING FACTOR (> 10^{21})

★ NEW SITUATION WITH LOW-Z MATERIALS

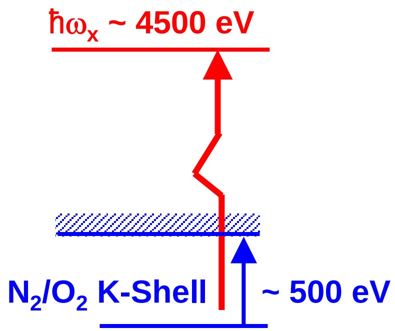

- High Energy 4.5 keV > 300 Ry > $\alpha m_e c^2$
- High Speed $\tau_x \sim < 10^{-17}$ s < $\hbar/\alpha^2 m_e c^2 \sim 24$ as
- High Intensity $I_x \sim 10^{26}$ W/cm^2, $E_x \sim 10^5$ e/a_o^2
- $r_x \leqslant \lambda_x \sim 5\, a_o$ (molecular scale)

★ Enables the creation of new compact ordered states of matter

★ Control e^- Motions

EXPERIMENTAL CONFIGURATION

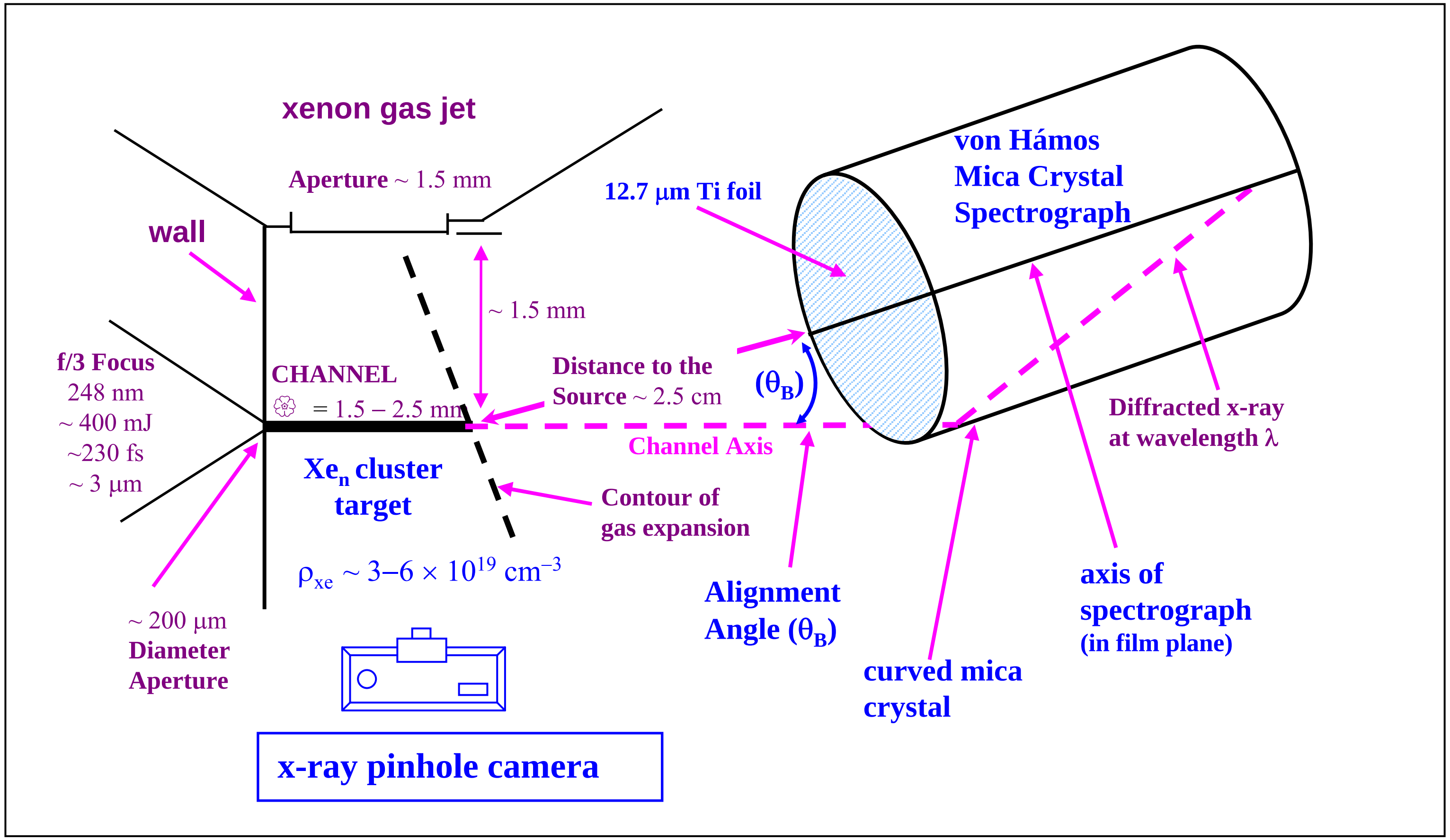

Fig. (2): Experimental configuration used for the observation of amplification of Xe(L) radiation in self-trapped channels inside an evacuated chamber. The x-ray pinhole camera was equipped with a ~ 10 μm thick Be foil enabling the morphology of the channel to be visualized by the Xe(M) emission (~ 1 keV). The observed channel length typically is ❁ ≅ 1.5–2.5 mm. The wall defining the entrance plane having the 200 μm aperture was fabricated from ~ 100 μm thick steel and the incident 248 nm pulse was focused with an f/3 off-axis parabolic optic to a spot size of ~ 3 μm. The entrance of the von Hámos spectrograph viewing the forward directed emission was protected with a Ti foil of 12.7 μm thickness whose transmission factor in the 2.7–3.0 Å region is ~ 0.5. The Bragg angle for the Xe^{34+} component at 2.88 Å is $\theta_B \cong 26°$. The film plane, which lies on the axis of the instrument, does not have a direct path to the x-ray source and, hence, only receives exposure by diffraction from the curved mica crystal. An identical von Hámos spectrograph, equipped with Muscovite mica from the same cut, was also used to record the spontaneous emission emitted transversely with respect to the channel axis. Not shown is the location of a film pack used for measurement of the amplified x-ray beam composed of a 2 cm square 12.7 μm thick Ti foil backed by a matching piece of x-ray film. With removal of the axial von Hámos spectrograph, this detector was placed on the channel axis in a perpendicular orientation at a distance of 12.5 cm from the cluster target.

Input Variable

Chamber Setup

Experimental Data Source

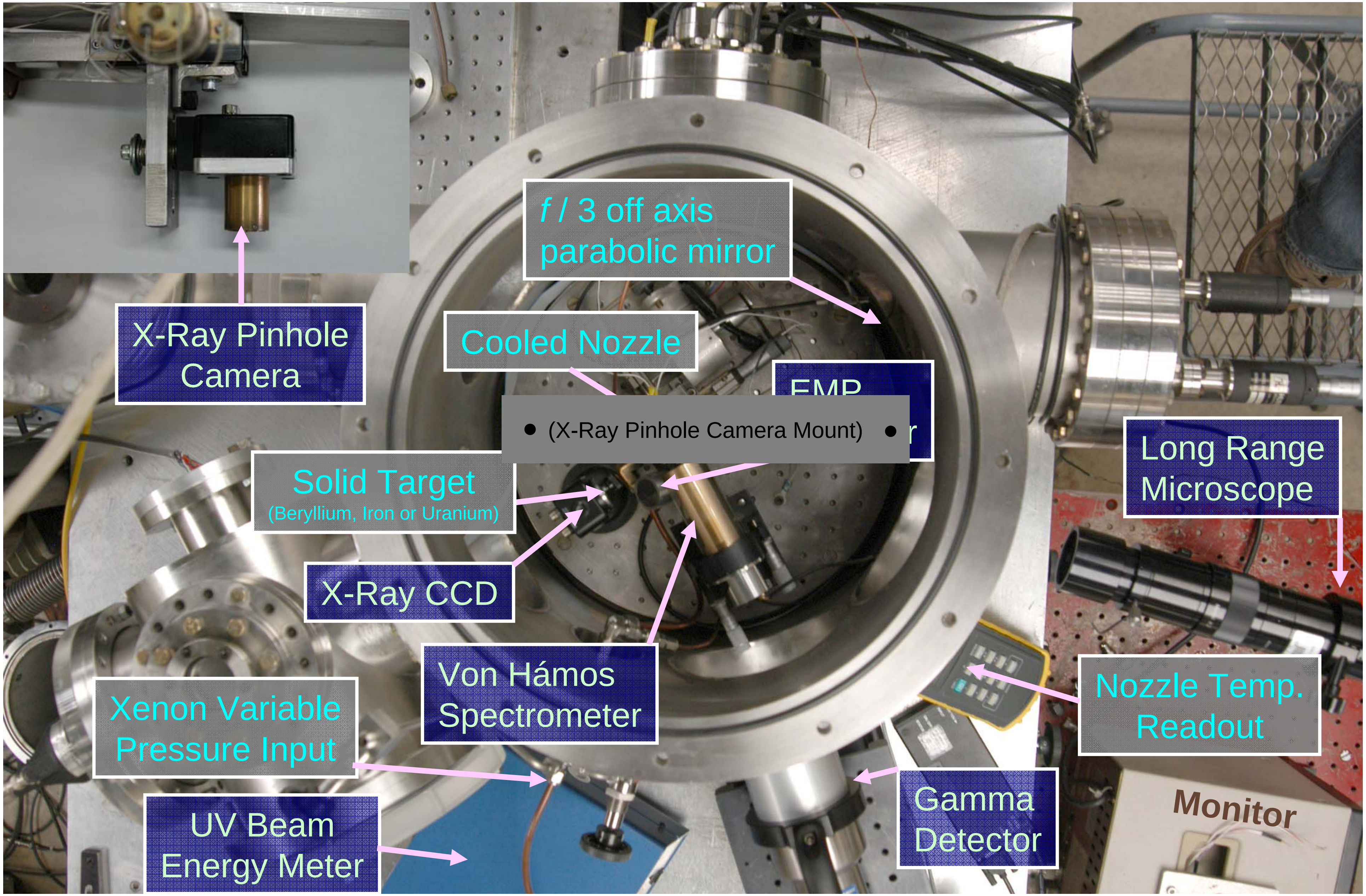

Experimental Setup

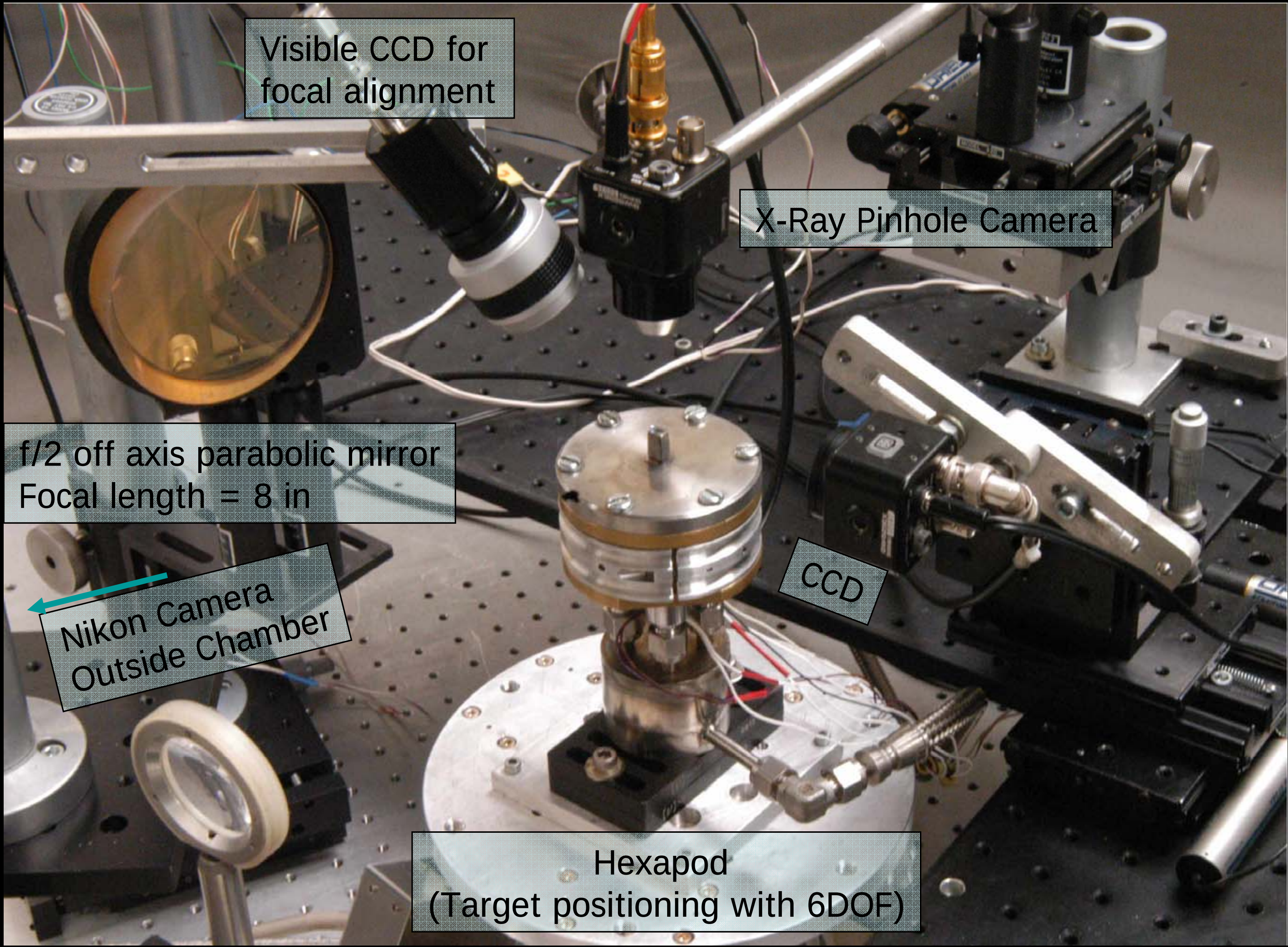

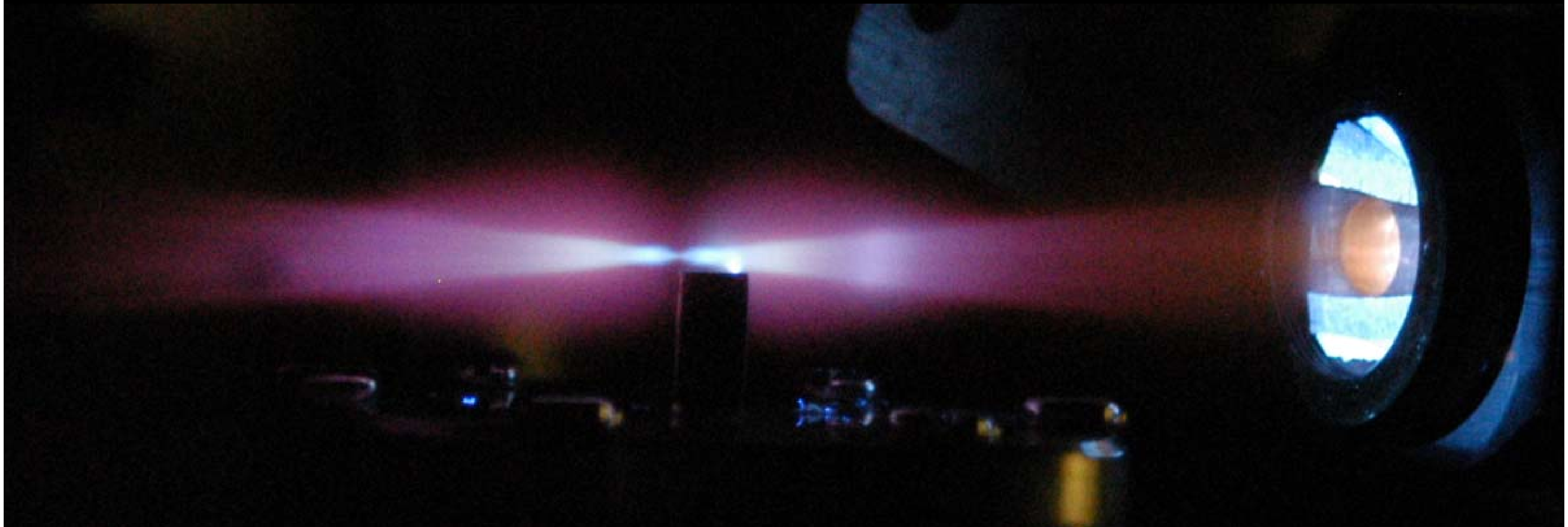

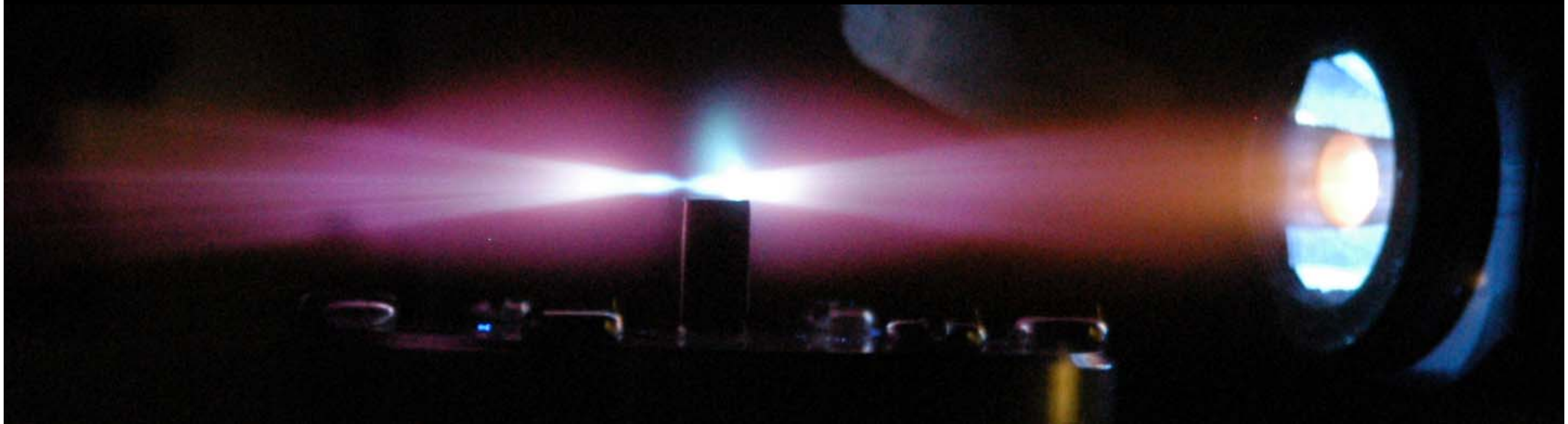

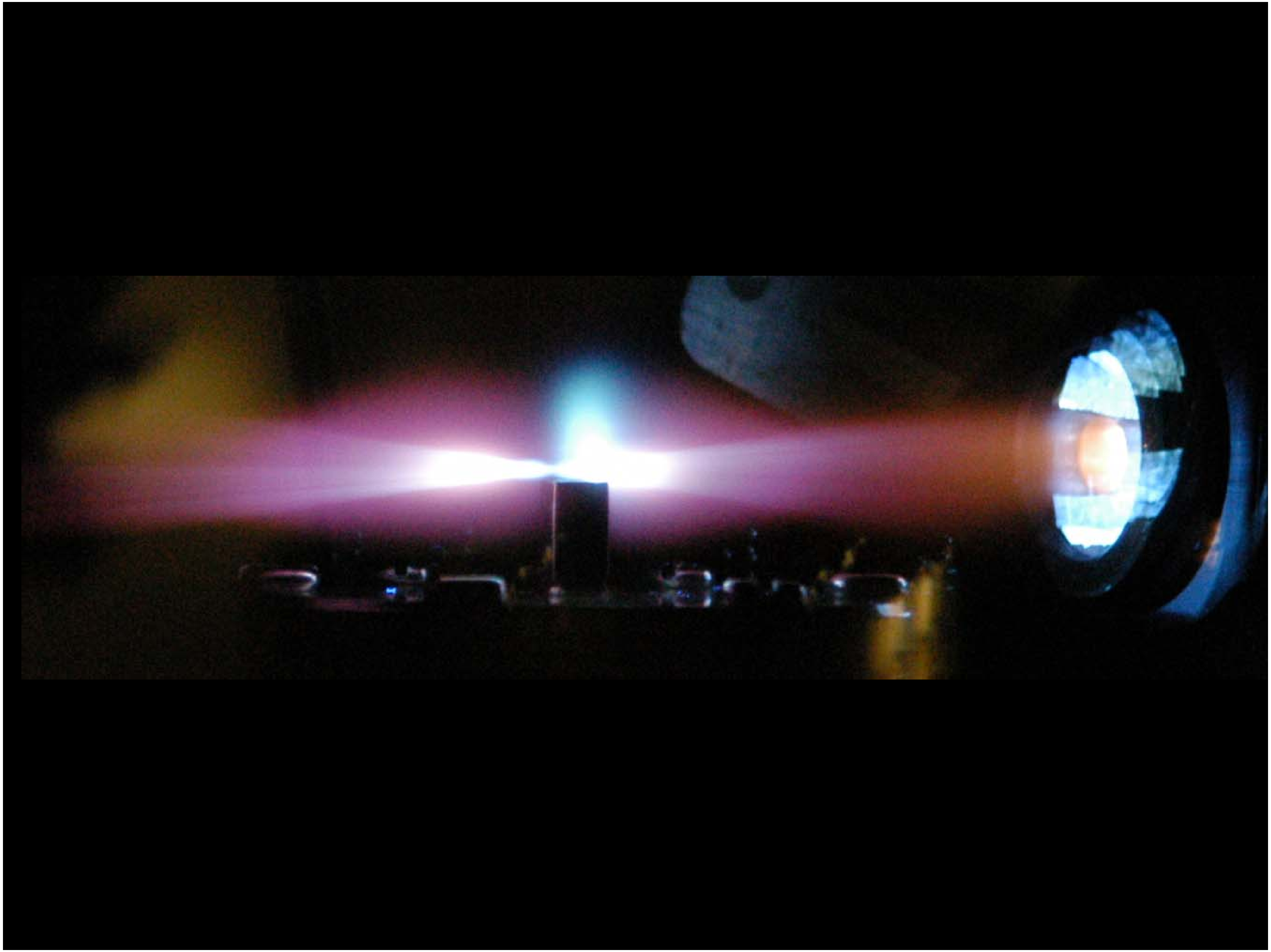

CHANNEL MORPHOLOGY
Xe(M) ~ 1 keV IMAGE

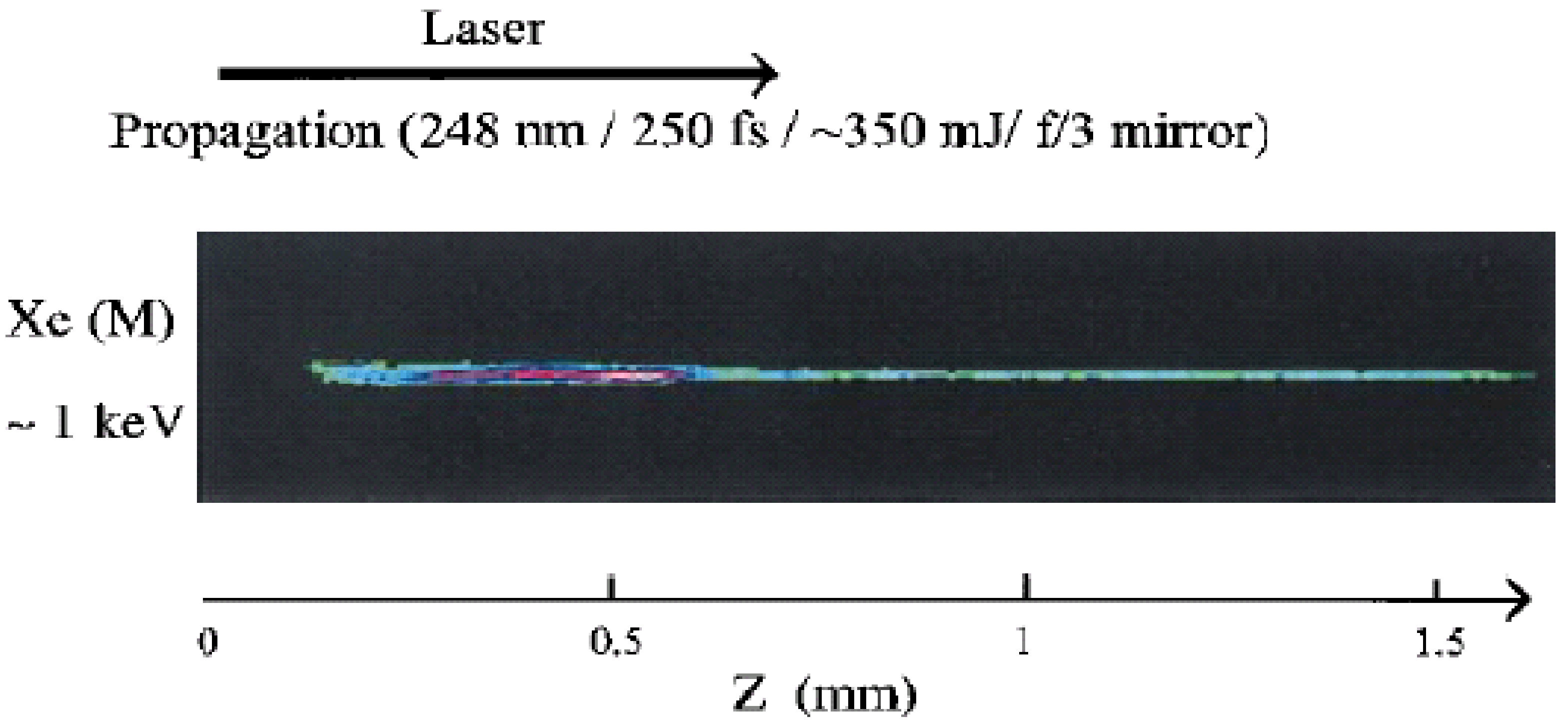

Xe(L) SPONTANEOUS EMISSION SPECTRUM

$2p^5 3d^n \rightarrow 2p^6 3d^{n-1}$

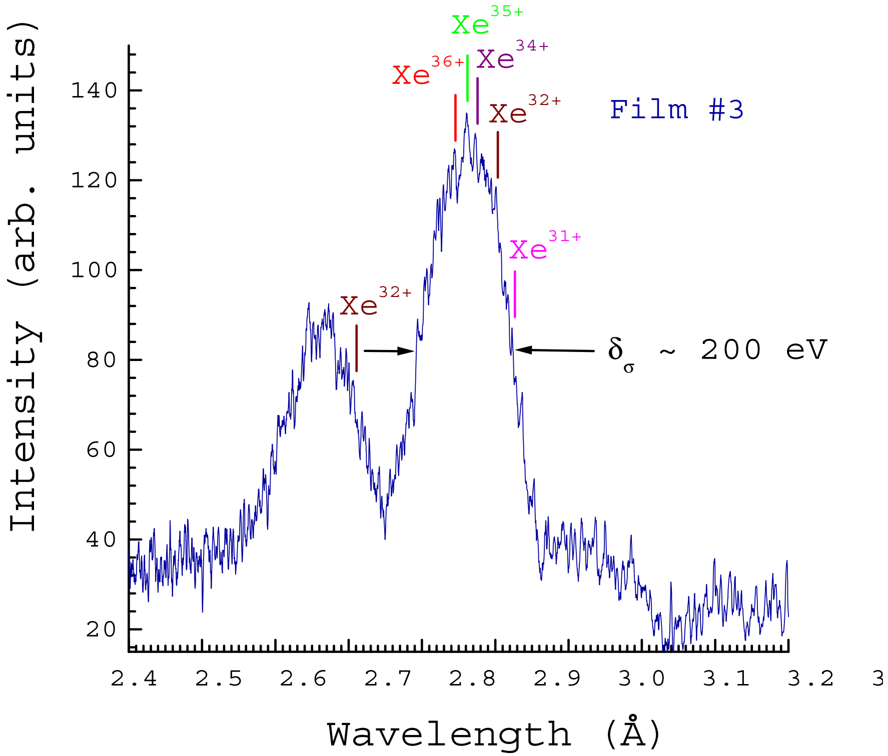

Fig. (1). Unamplified spontaneous emission profile of the Xe(L) 3d–2p hollow atom [7] spectrum (film #3) produced from Xe clusters with femtosecond 248 nm excitation <u>without</u> plasma channel formation. The splitting between the major and minor lobes arises from the spin-orbit interaction of the 2p vacancy. The full width of the main feature is δ_σ ~ 200 eV. The positions of selected charge state transition arrays (Xe^{31+}, Xe^{32+}, Xe^{34+}, Xe^{35+}, and Xe^{36+}) are indicated.

Xe(L) Amplification

Xe(L)

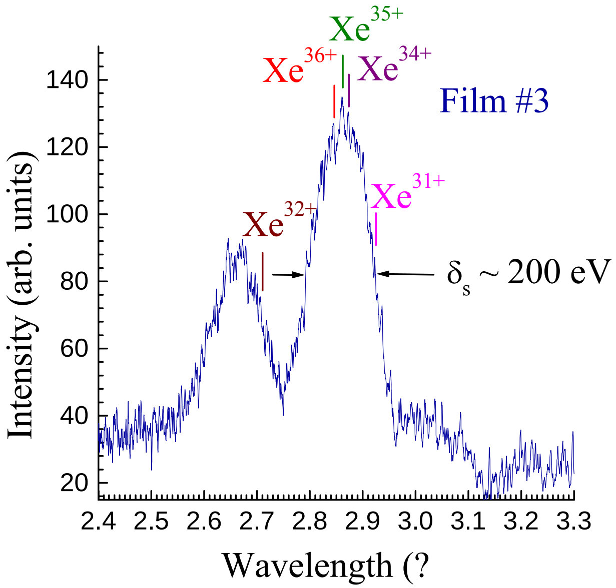

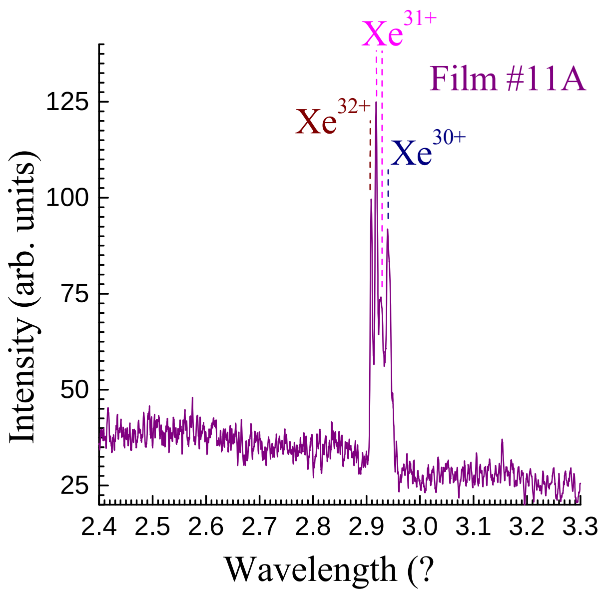

Ruby

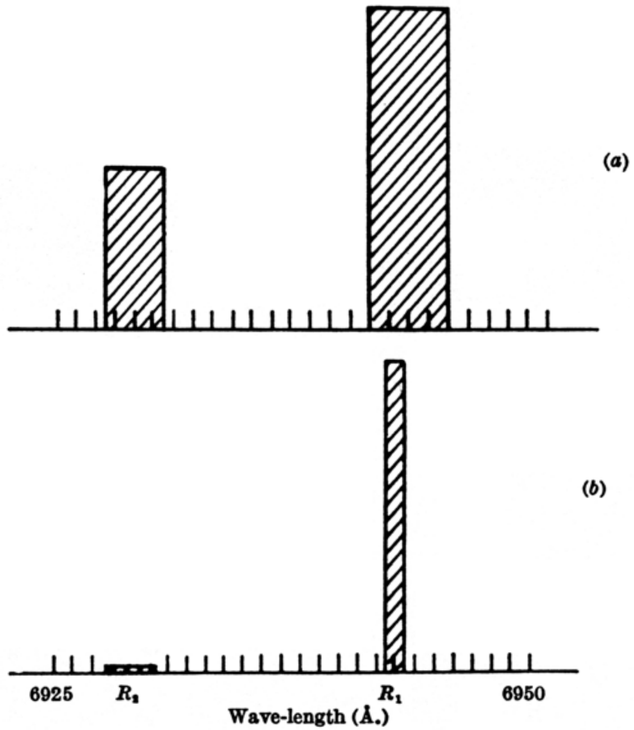

Fig. 2. Emission spectrum of ruby: *a*, low-power excitation; *b*, high-power excitation

the emission spectrum obtained under these conditions is shown in Fig. 2*b*. These results can be explained on the basis that negative temperatures were produced and regenerative amplification ensued. I expect, in principle, a considerably greater ($\sim 10^8$) reduction in line width when mode selection techniques are used[1].

I gratefully acknowledge helpful discussions with G. Birnbaum, R. W. Hellwarth, L. C. Levitt, and R. A. Satten and am indebted to I. J. D'Haenens and C. K. Asawa for technical assistance in obtaining the measurements.

T. H. Maiman

Hughes Research Laboratories,
A Division of Hughes Aircraft Co.,
Malibu, California.

Xe^{34+} Line Amplification

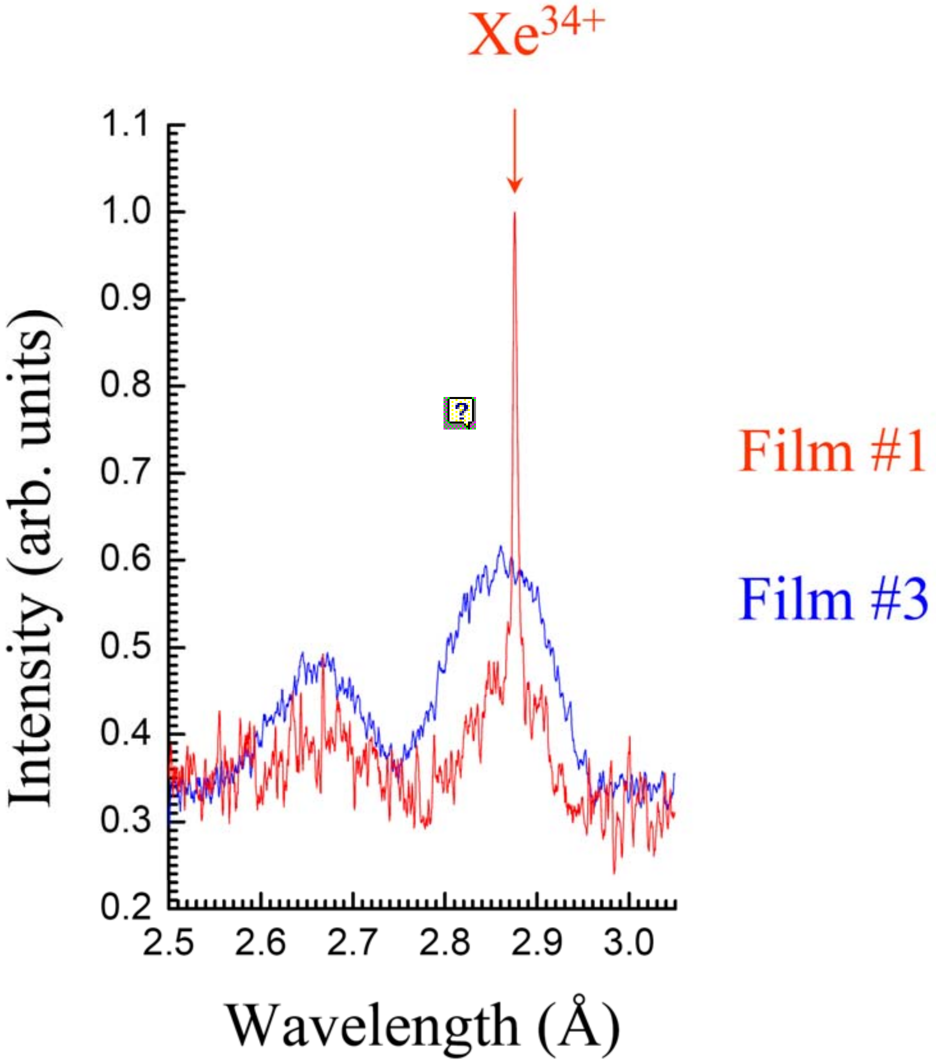

Amplified X-Ray Spectrum

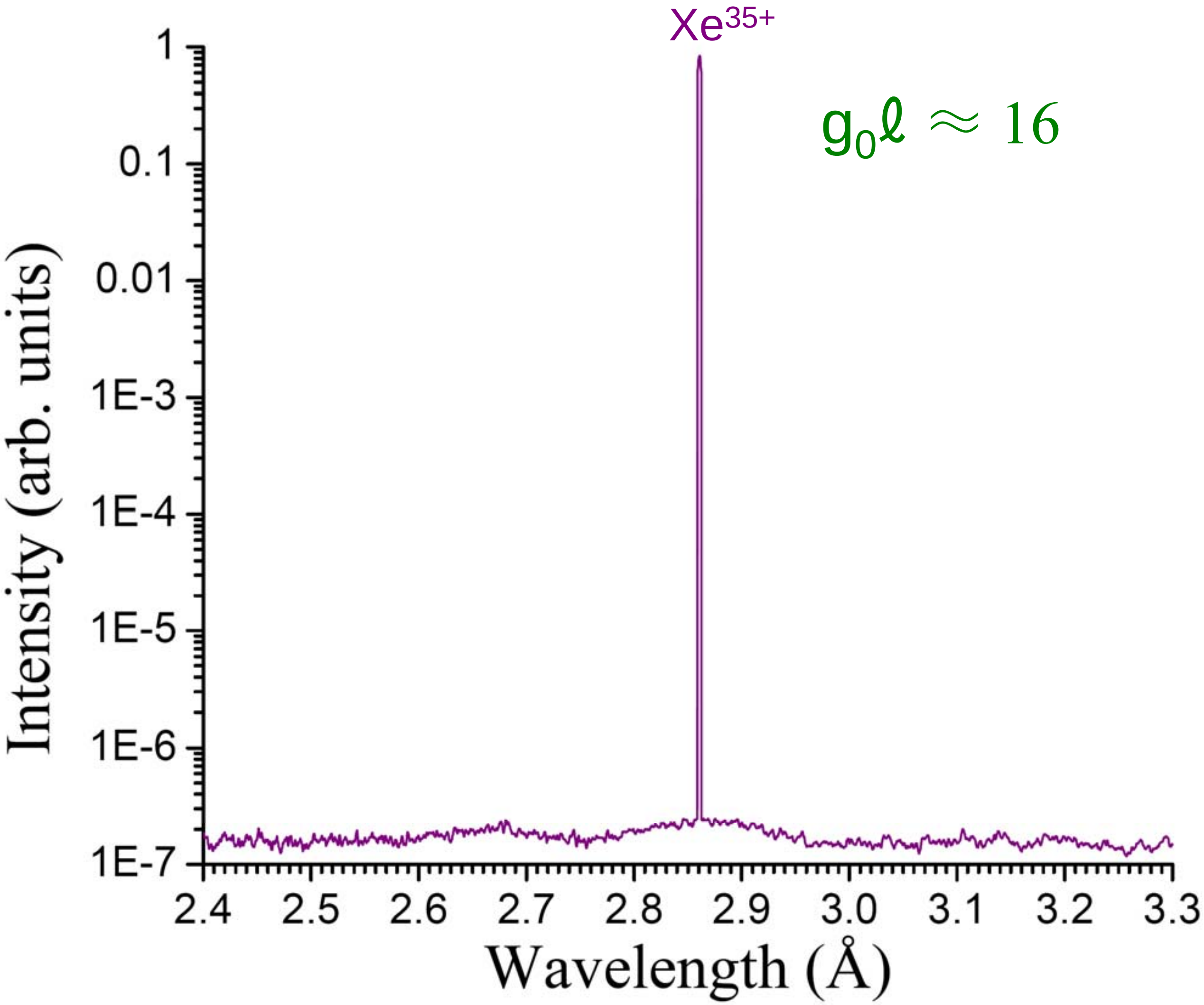

Xe(L) AMPLIFICATION / Xe^{32+} ~ 2.71 Å

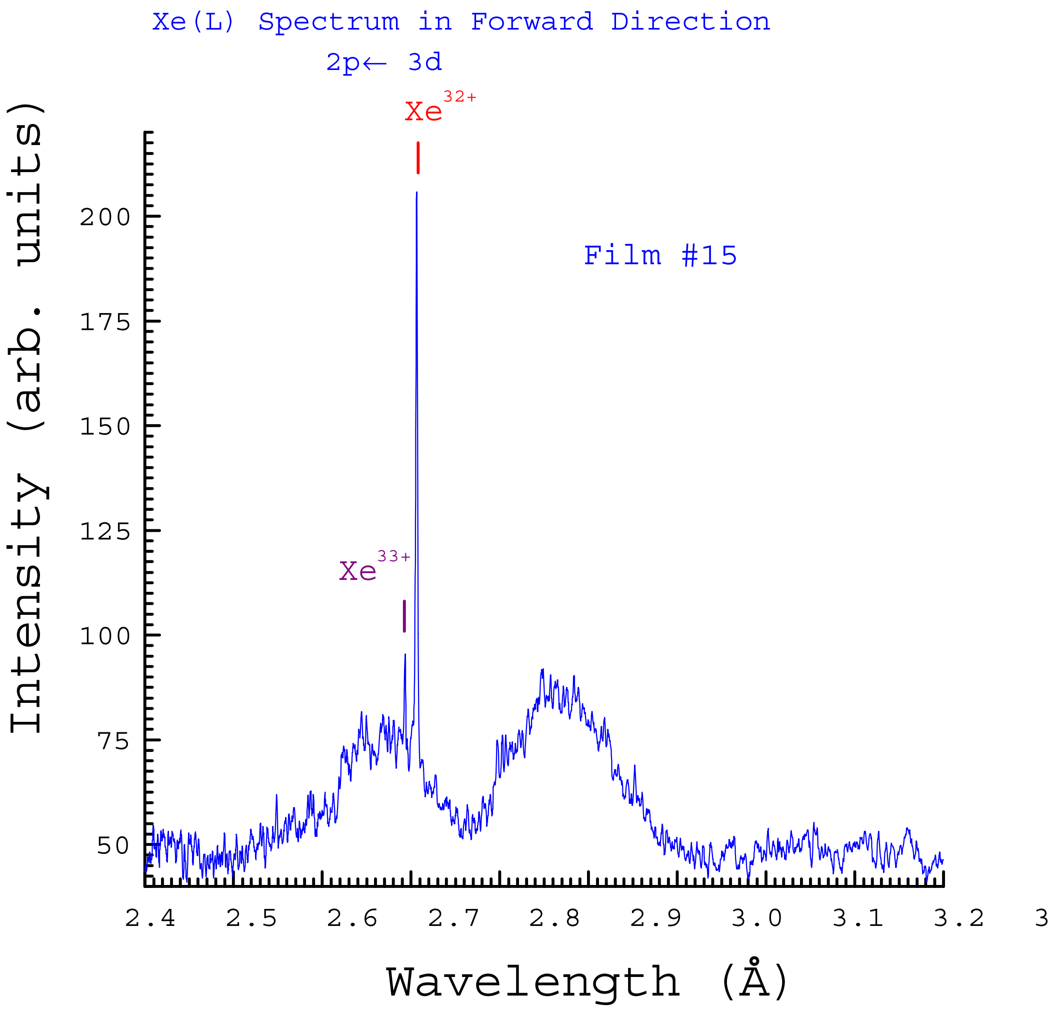

Xe^{32+} (2.7 Å) Film Focus

Film #15

$d_1 \cong 60\ \mu m$

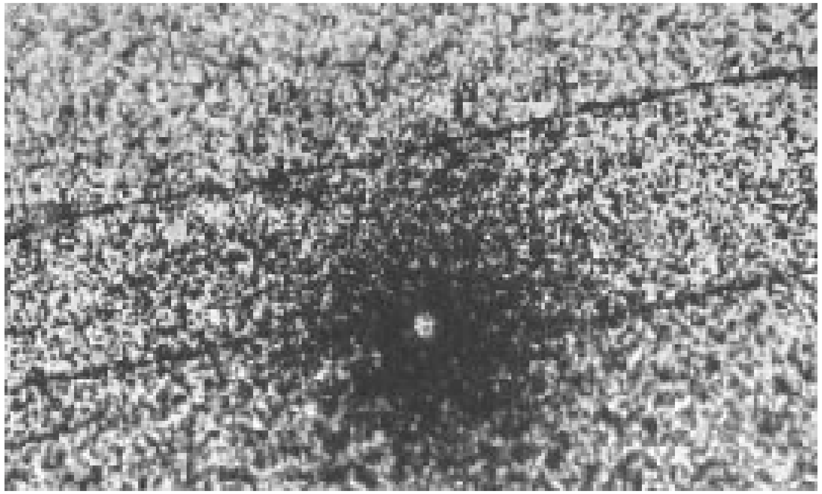

$d_2 \cong 5\ \mu m$

Single-Pulse Observation of Xe(L) Spectrum in Transverse Direction

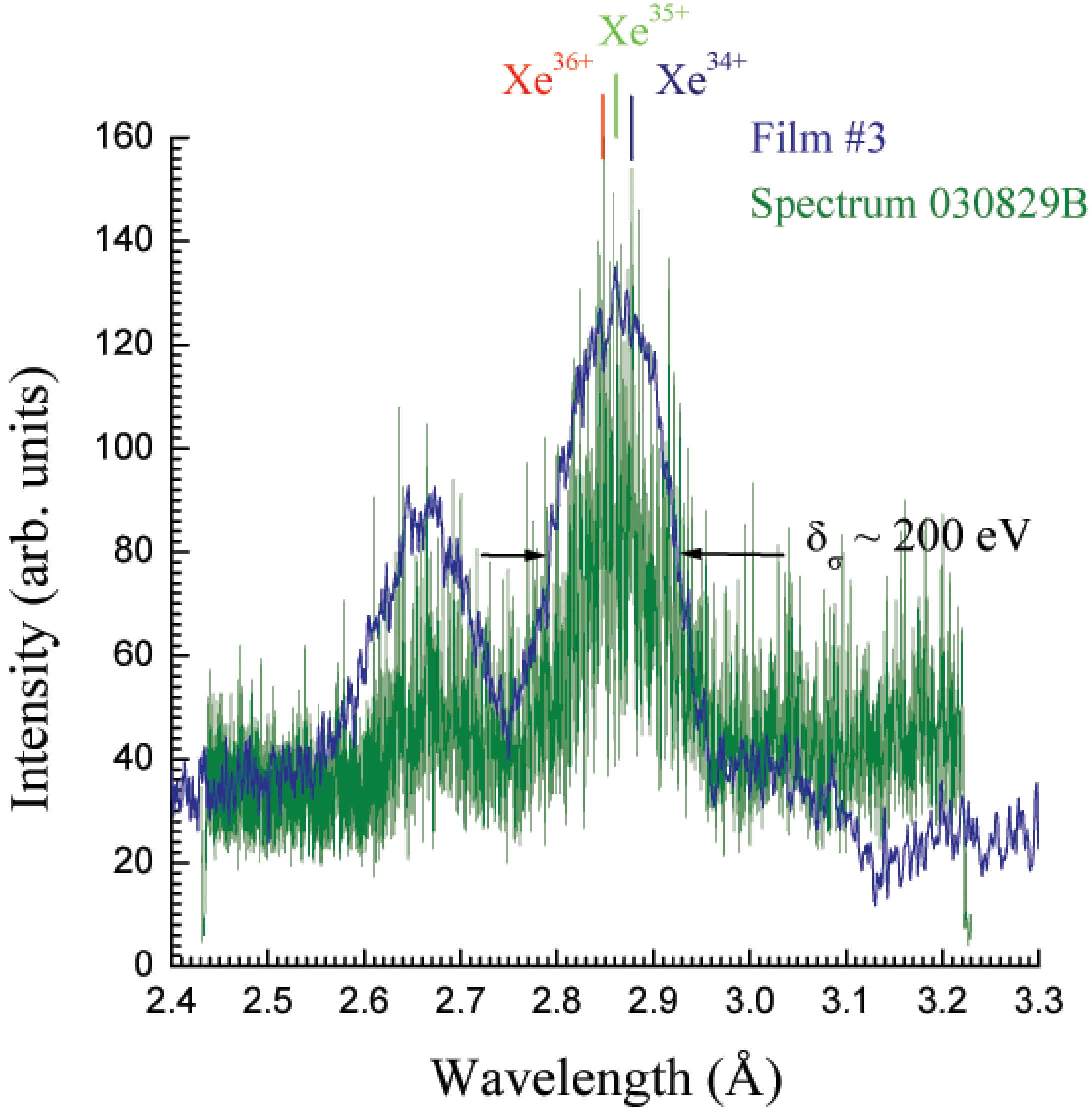

UIC / Alex B. Borisov, Keith Boyer, and Charles K. Rhodes, 09/03/2003

Characteristic Unamplified Single-Pulse and Time-Integrated Spontaneous Emission Xe(L) Spectra

Characteristic Unamplified Axial Single-Pulse Xe(L) Spectrum

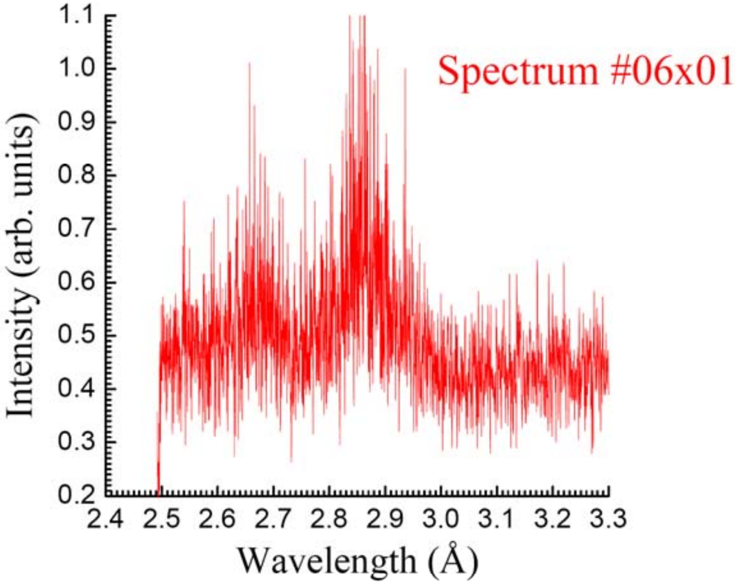

Characteristic Unamplified Axial Single-Pulse and Transverse Time-Integrated Xe(L) Spectra

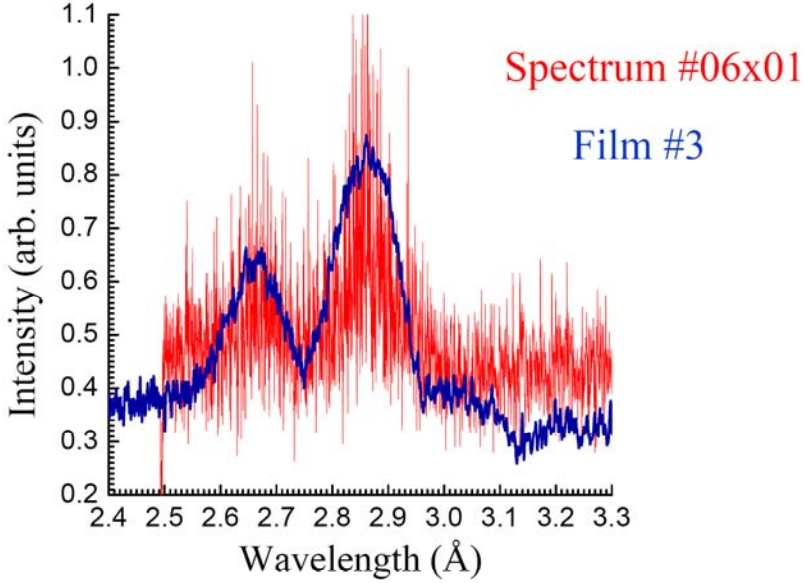

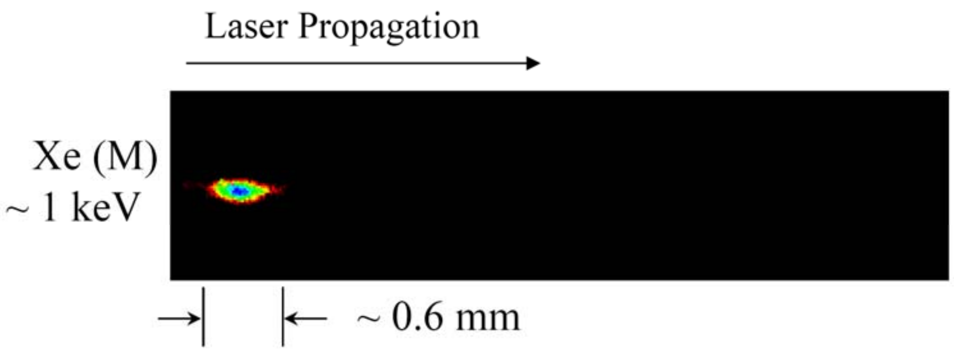

Propagation Image #06x01

No Channel Formation

SINGLE-PULSE (CCD) CONFIRMATION OF SPECTRAL HOLE-BURNING

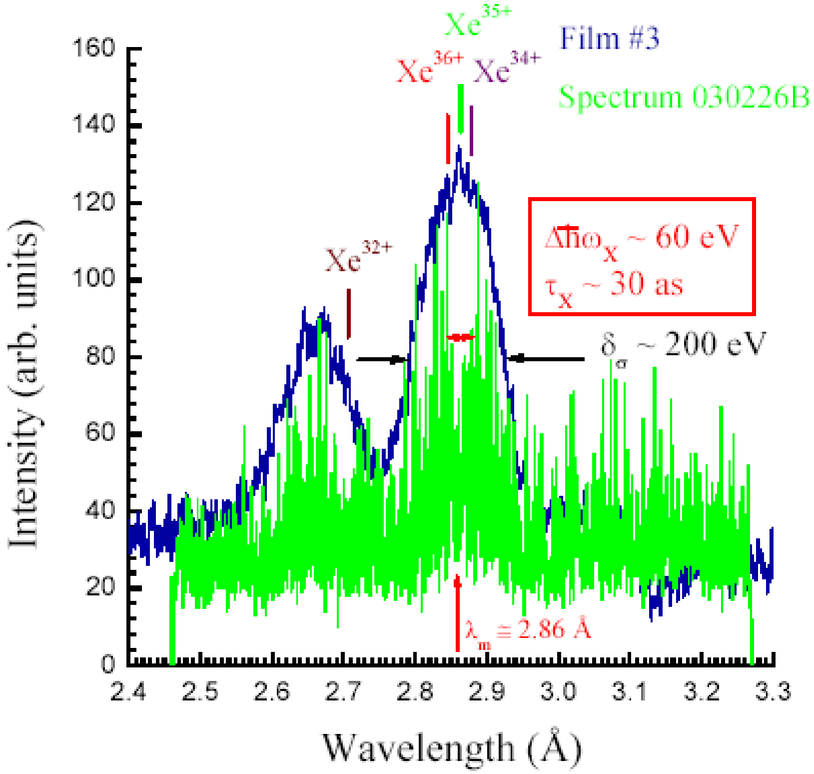

Fig. (3): Comparison of the characteristic spontaneous Xe(L) hollow atom emission spectrum (film #3) shown in Fig. (1) with a corresponding single-pulse spectrum (#030226B) recorded in a direction transverse to the channel. The principal feature of this comparison is the presence of a deep and broad ($\Delta\hbar\omega_x \sim 60$ eV) spectrally hole-burned gap that matches well the location of the Xe^{34+} and Xe^{35+} arrays and is centered at $\lambda_m \cong 2.86$ Å, the wavelength at which complete suppression of the transversely radiated emission is observed. The width $\Delta\hbar\omega_x$ corresponds to a bandwidth sufficient for the amplification of multikilovolt x-ray pulses down to a limiting width $\tau_x \sim 30$ as. An additional zone of spectral hole-burning is apparent near $\lambda \cong 2.7$ Å. This region is associated with the Xe^{32+} array on the minor lobe that exhibited very strong amplification in the earlier study [8]. The spectral resolution of the CCD recorded data is estimated to be ~ 4 eV.

- **Full Signal Extinction at $\lambda_m \sim 2.86$ Å (Xe^{35+})**
- **Spectral Width $\Delta\hbar\omega_x \sim 60$ eV $\Rightarrow$ ~ 30 as (Atomic Time $\hbar/m_ec^2 \sim 24$ as)**

Xe(L) Saturated Amplification Spectral Width Measurement

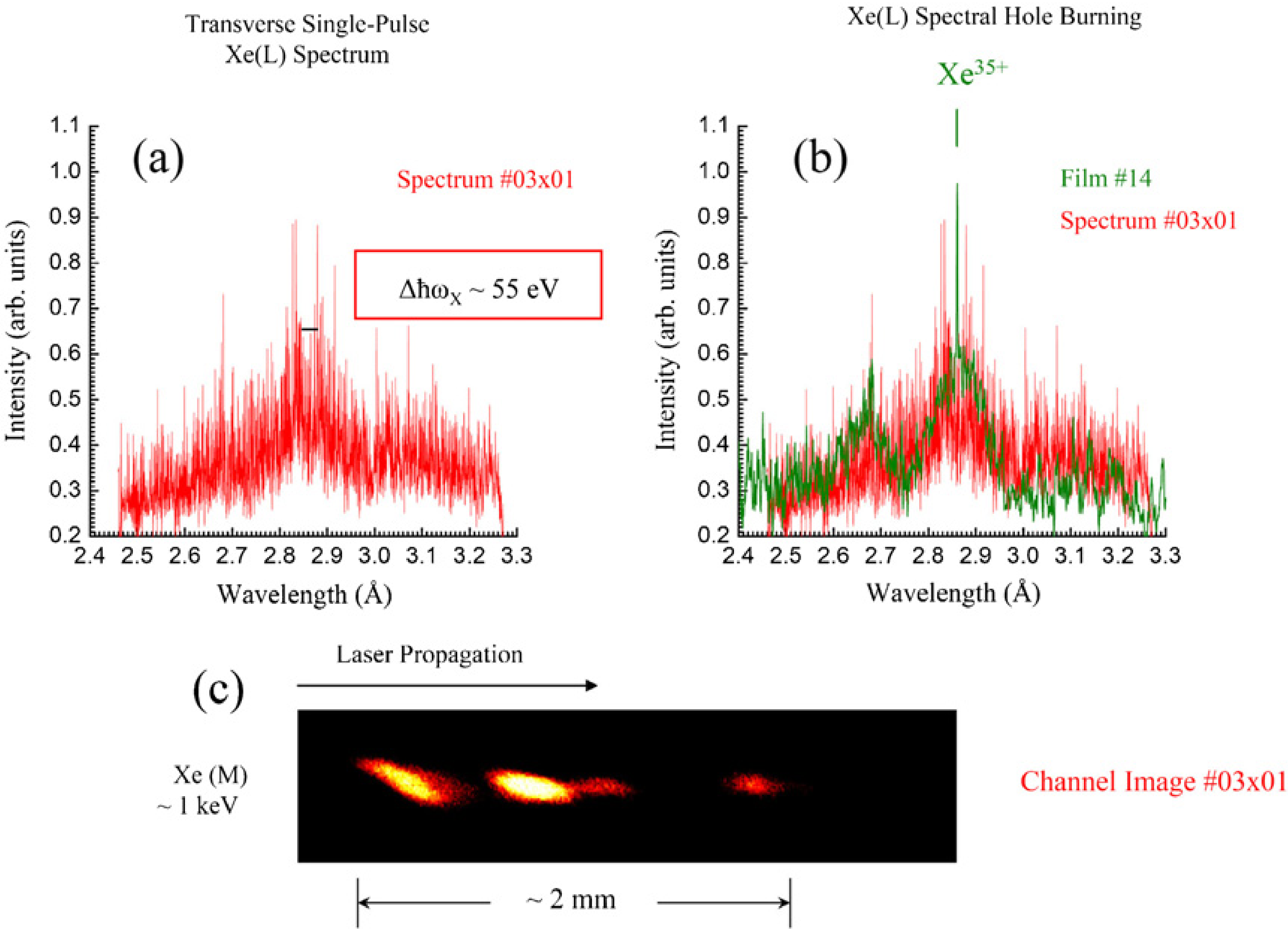

Axial Amplified Single-Pulse and Time-Integrated Xe(L) Spectra

Axial Single-Pulse Xe(L) Spectrum

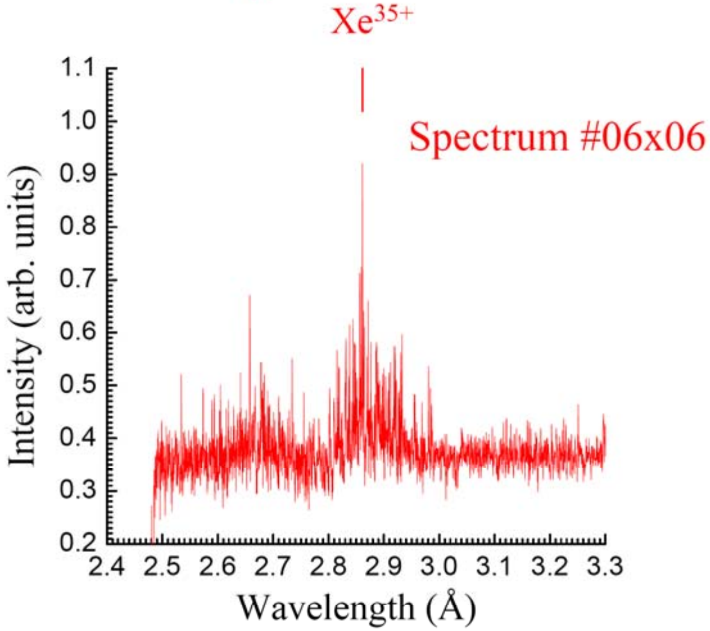

Axial Single-Pulse and Time-Integrated Spectra

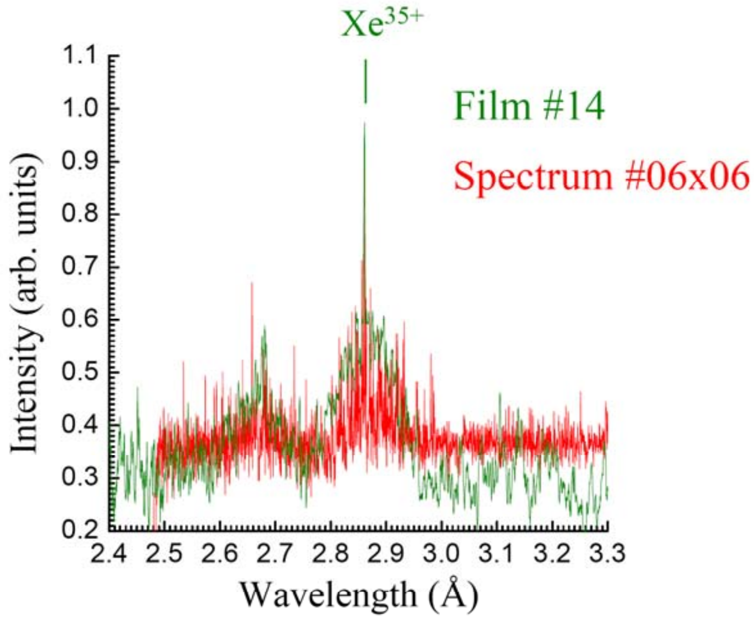

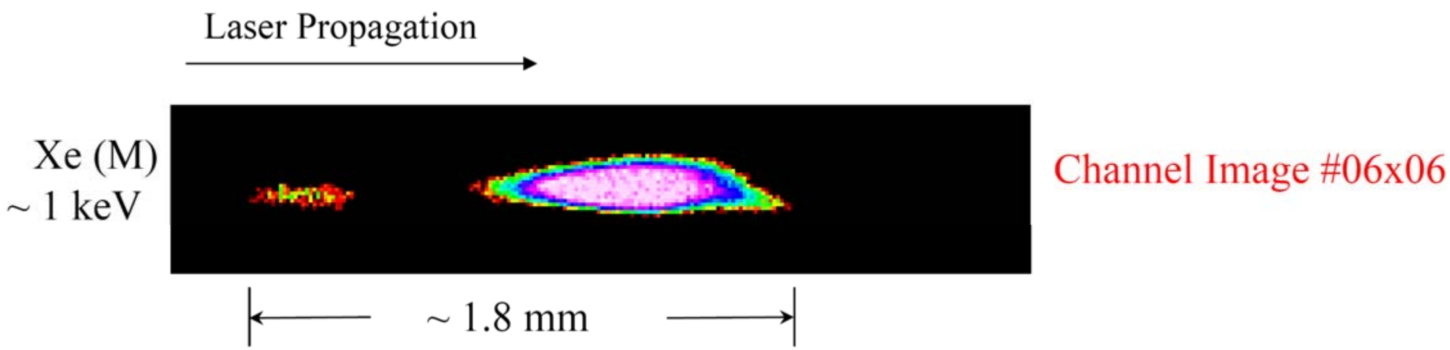

Axial Amplified Single-Pulse and Time-Integrated Xe(L) Spectra

Axial Single-Pulse Xe(L) Spectrum

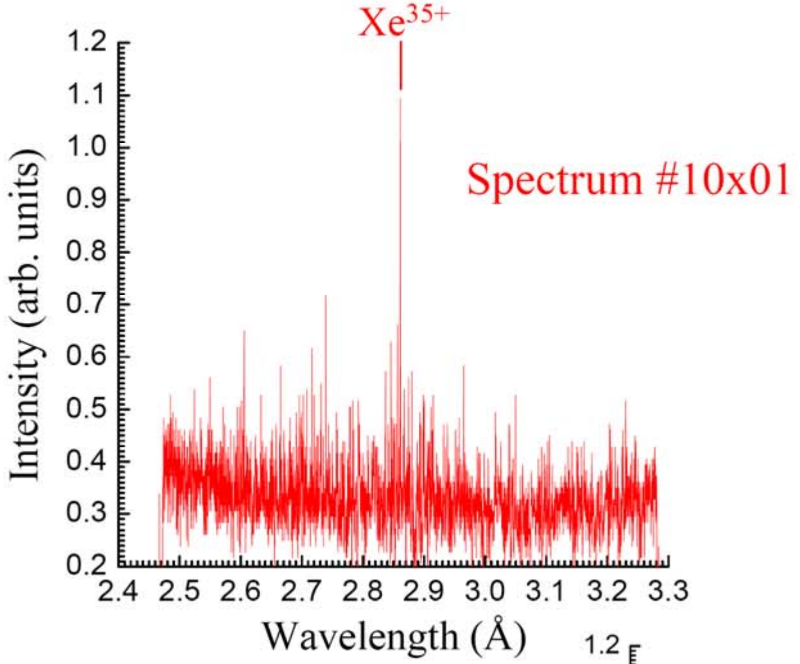

Axial Time-Integrated Spectrum

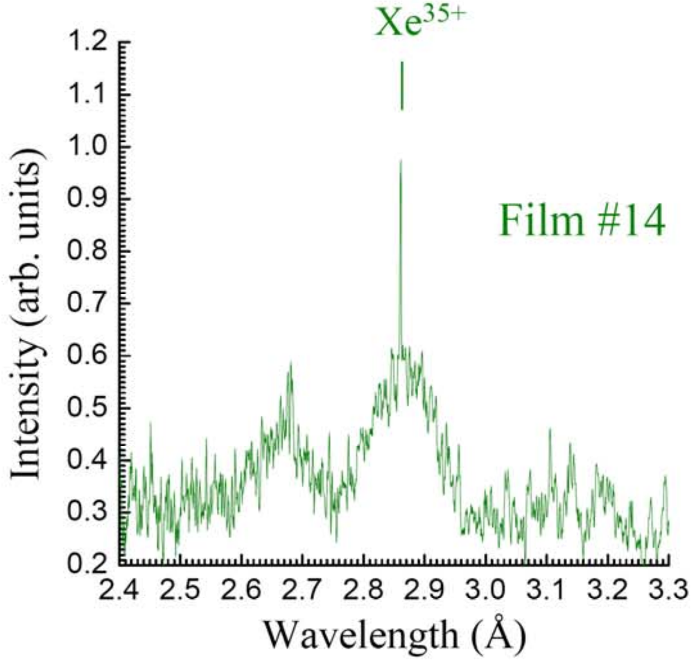

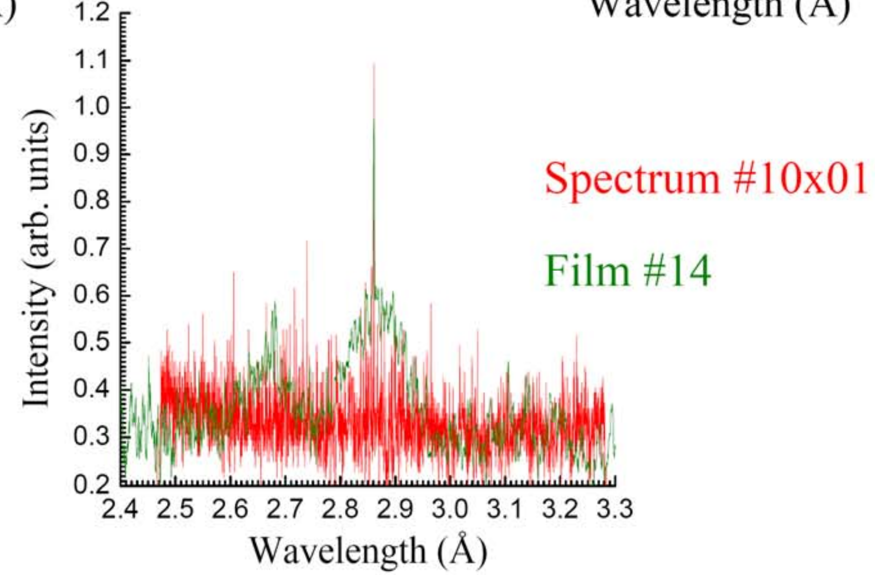

Axial Amplified Single-Pulse and Time-Integrated Xe(L) Spectra

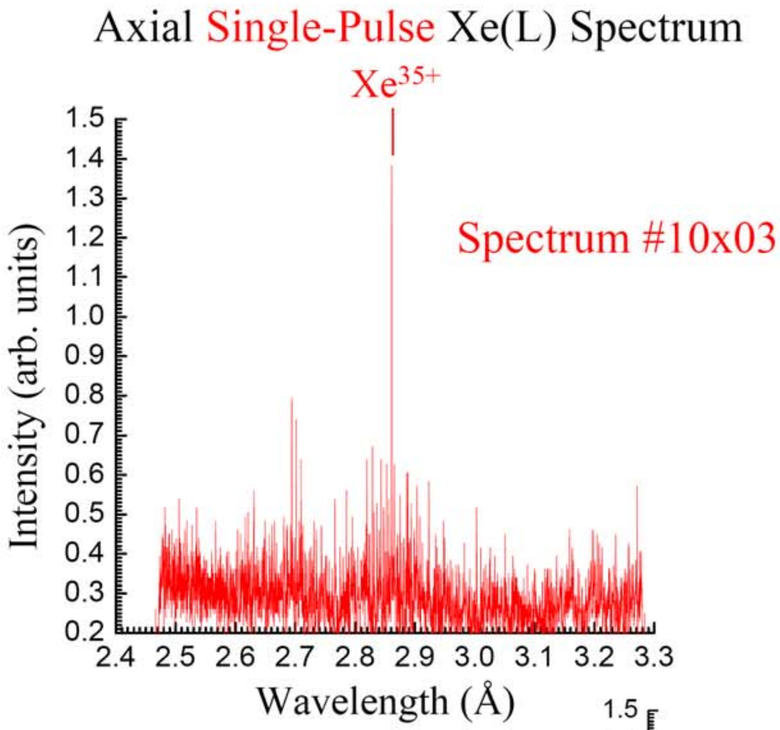

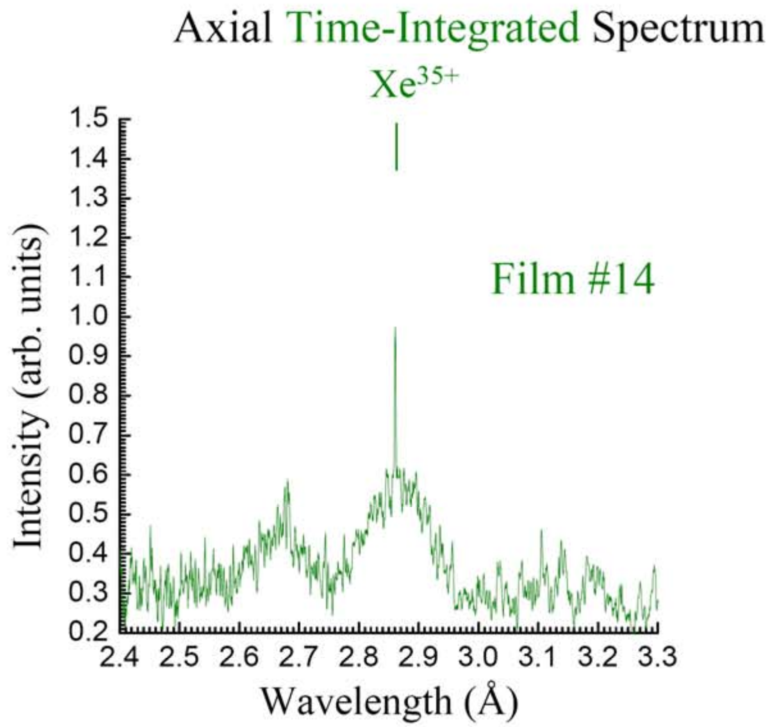

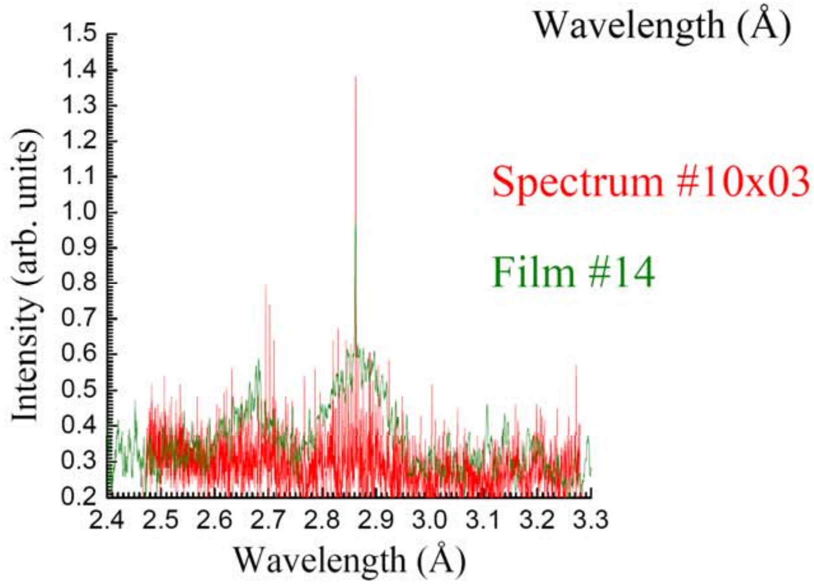

X-RAY BEAM DOUBLE VISION

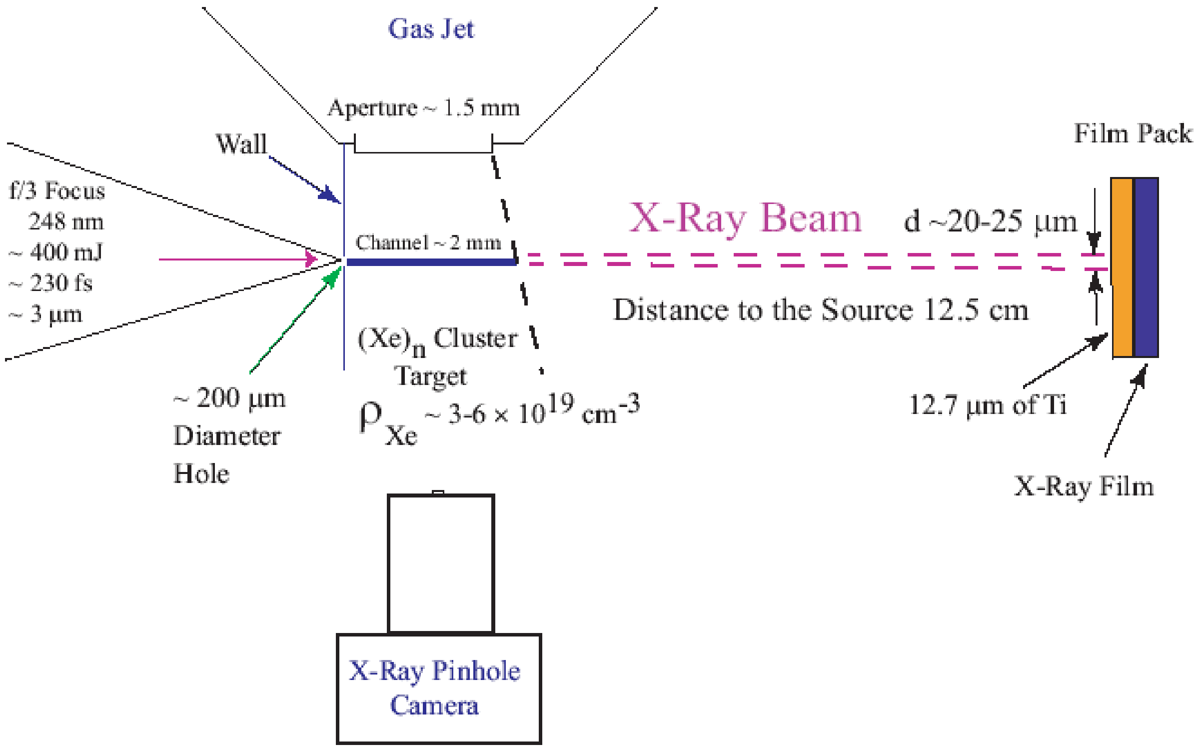

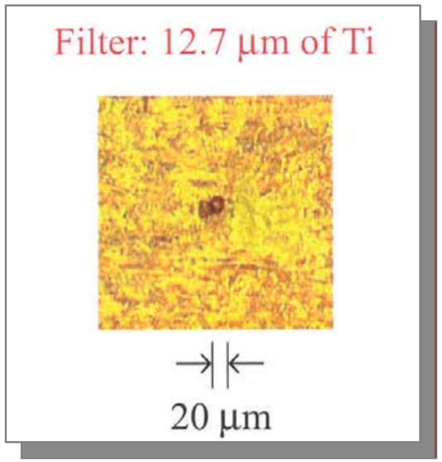

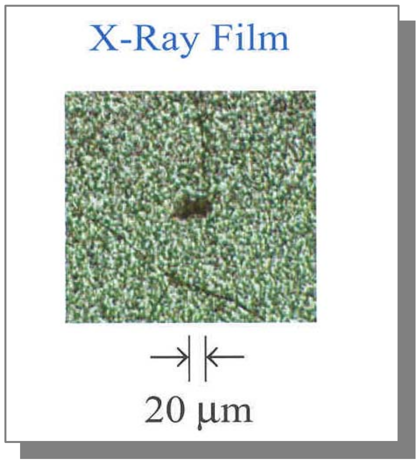

$\delta\theta_x \sim 200\ \mu r$

Experimental Data Xe(L) on Solid Targets

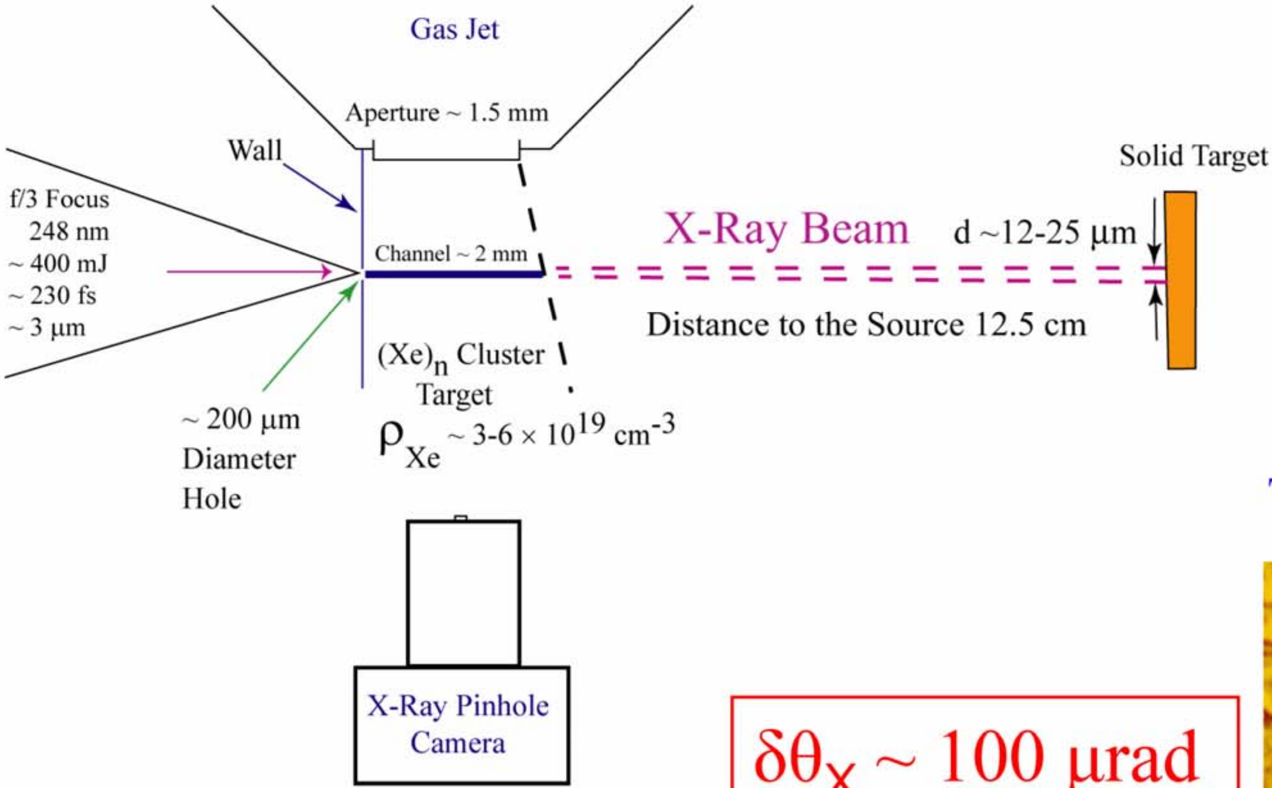

$\delta\theta_X \sim 100\ \mu rad$

Titanium Target

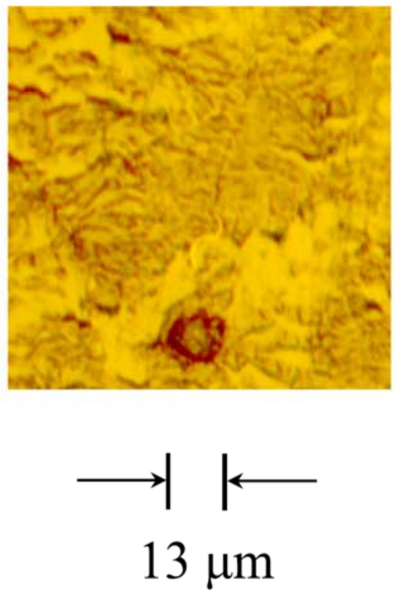

COOLED CLUSTER FORMATION

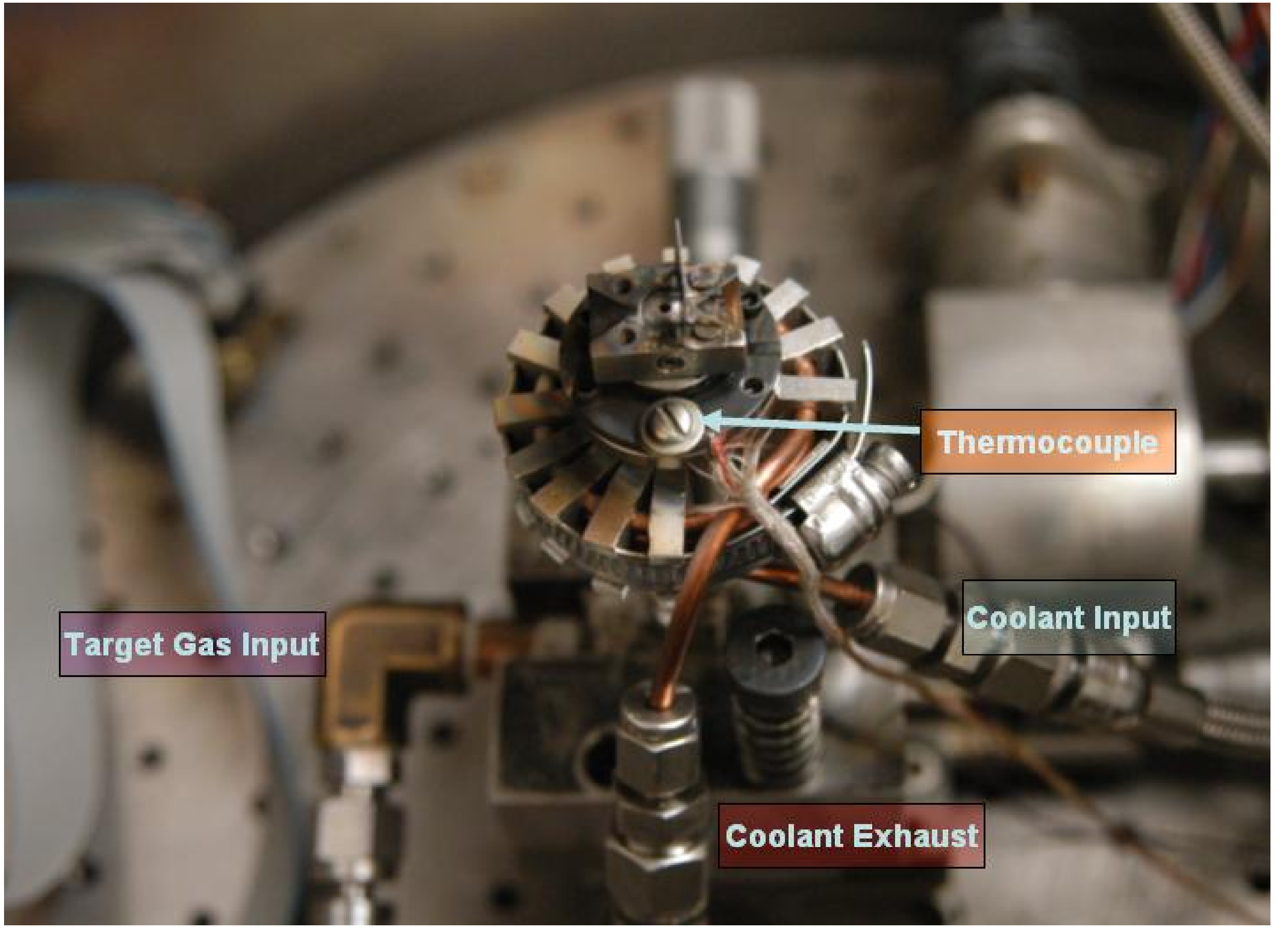

Picture of cooled Xe nozzle showing the coolant coil and the Xe target gas input. The temperature is measured with a thermocouple located on the body of the nozzle. The nozzle emits the xenon gas plume upward in this bird's-eye view.

Temperature Dependence of Xe(L) X-Ray Pulse Intensity

Single-Pulse Xe(L) Spectra in Forward Direction

(a)

Spectrum #32x01
$T = 297$ K
$E_{248} \cong 410$ mJ

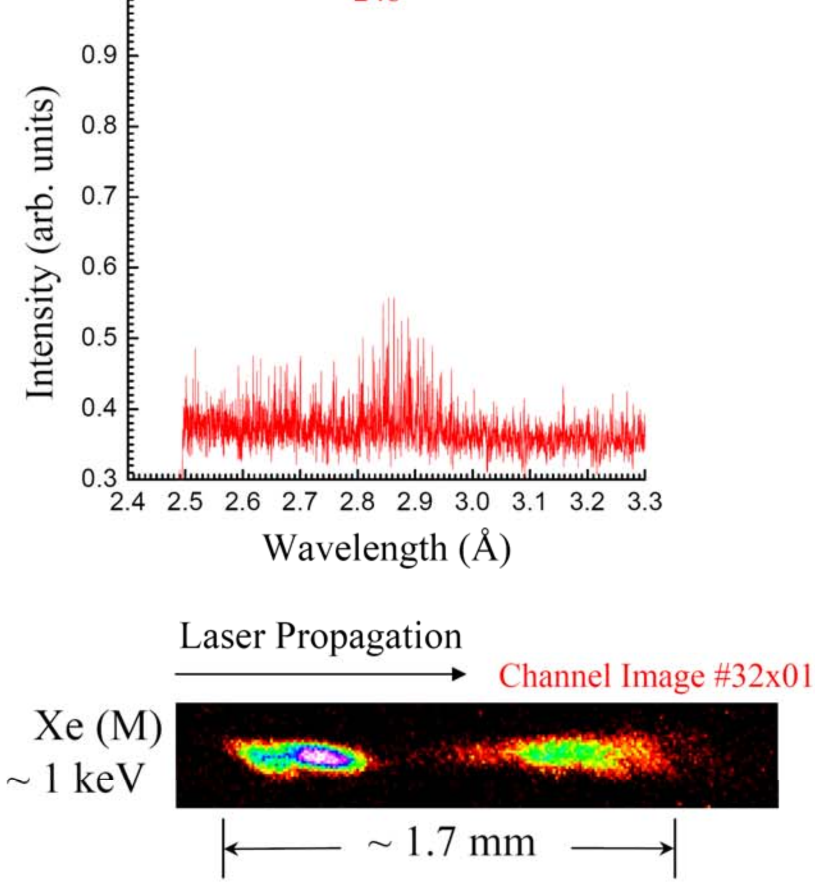

(b)

Spectrum #32x02
$T = 230$ K
$E_{248} \cong 400$ mJ

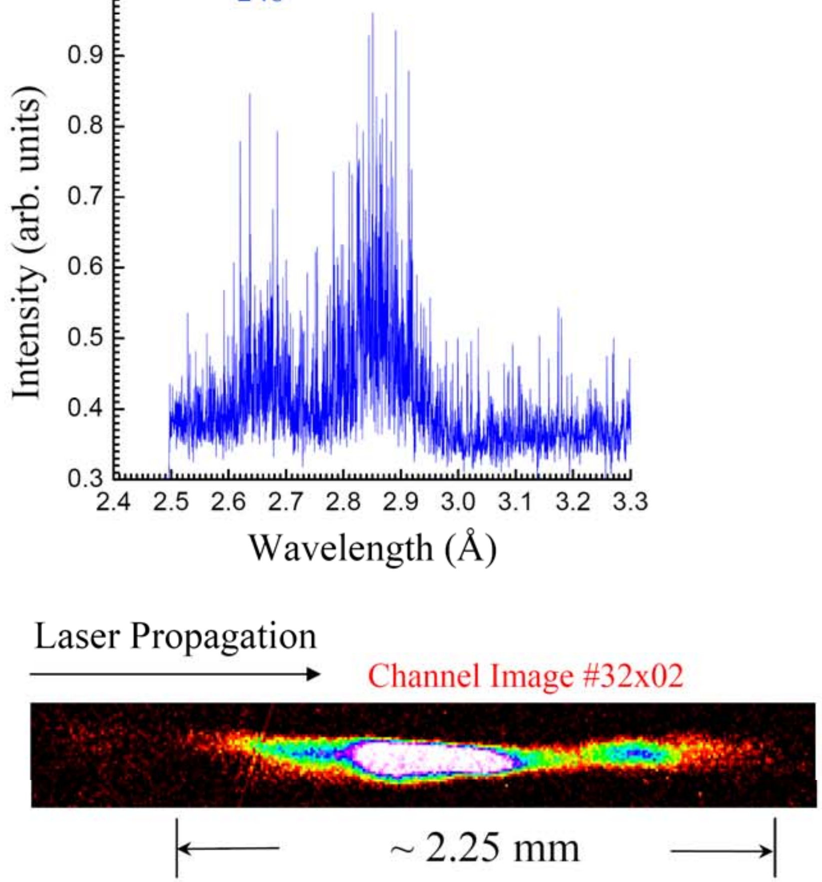

Temperature Dependence of Xe(L) X-Ray Emission Intensity

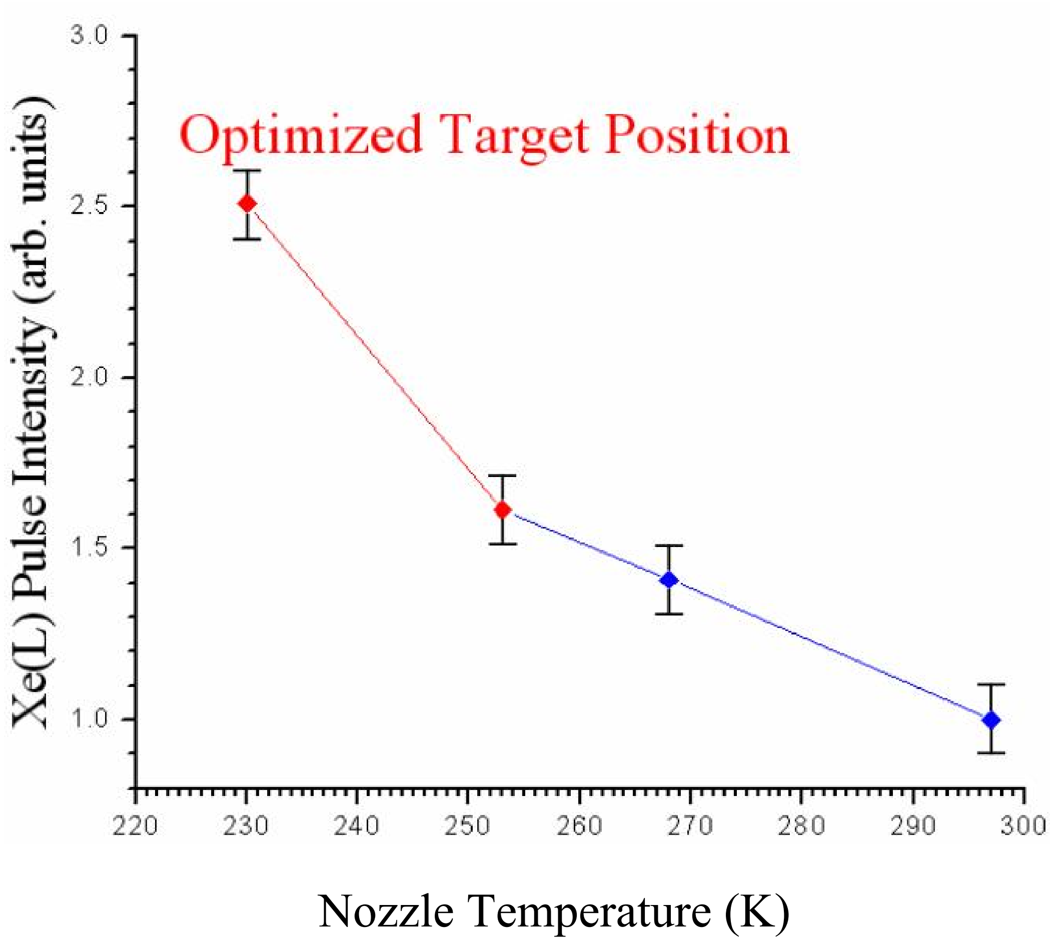

AMPLIFIER GAIN

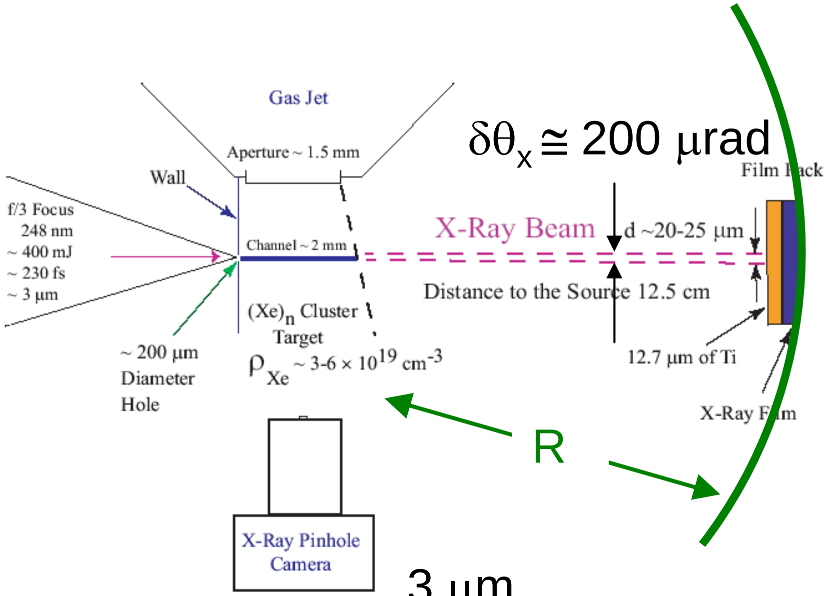

$\delta\theta_x \cong 200\ \mu\text{rad}$

$A_x \cong 4 \times 10^{-6}\ \text{cm}^2$

Ti

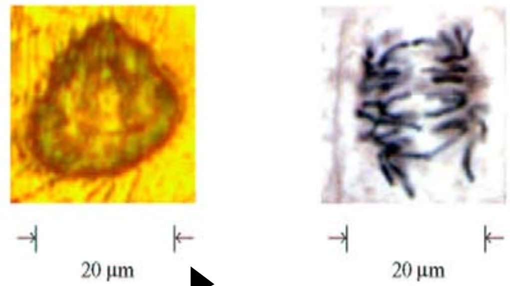

$E_x \geq 10\ \mu\text{J}$ (Damage)

3 μm

$E_{ch} = \frac{\pi d^2 \ell}{4} \rho\hbar\omega \leq 1\ \text{mJ}$

2 mm

$\delta\theta_{geom} \cong 1500\ \mu\text{rad}$

$A = 4\pi R^2 = 1962\ \text{cm}^2$ (R=12.5 cm)

$A/A_x \cong 4.9 \times 10^8$

Uniform 4π radiator $\rightarrow$
$\rightarrow E \sim E_x\,(A/A_x) \cong 4.9\ \text{kJ}$

$$\delta\theta_{geom} \cong \frac{3 \times 10^{-4}}{2 \times 10^{-1}} = 1.5 \times 10^{-3} = 1500\ \mu\text{rad} >> \delta\theta_x = 200\ \mu\text{rad}$$

measured

$$\text{Gain} = G \sim E/E_{ch} \cong \frac{4.9\ \text{kJ}}{1\text{mJ}} \cong 5 \times 10^6 \sim 1\text{–}5 \times 10^6$$

GAIN COMPARISONS

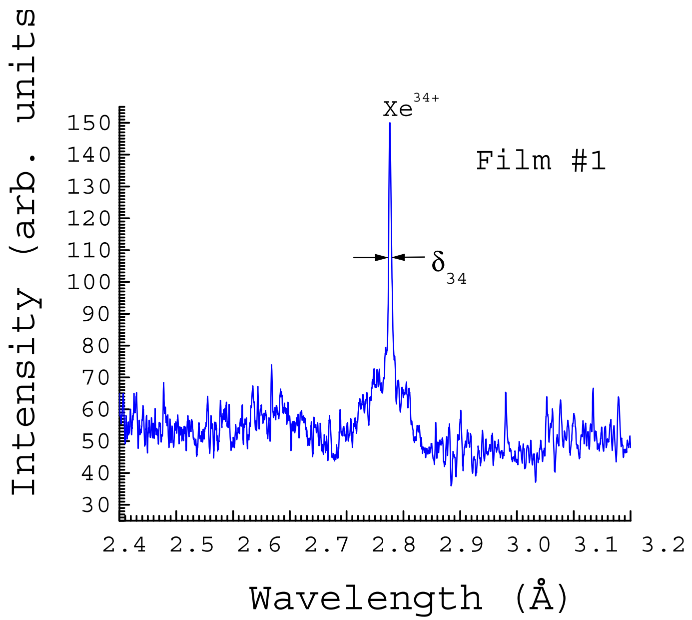

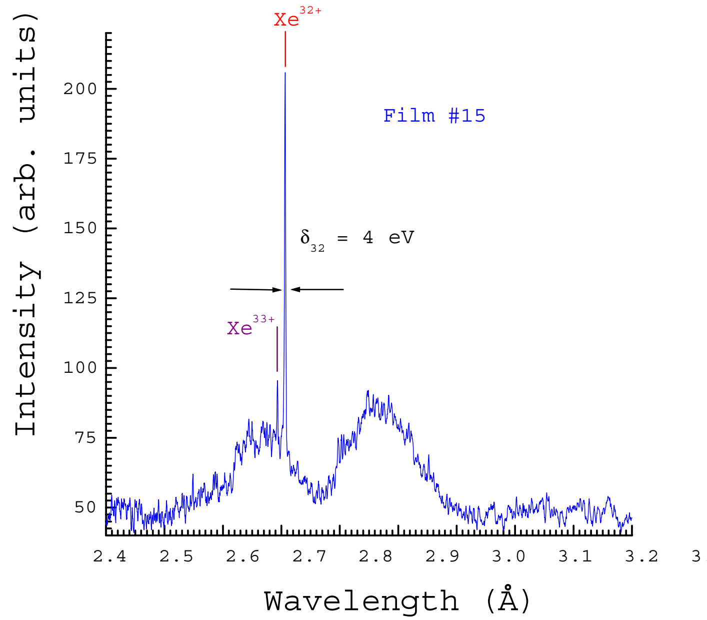

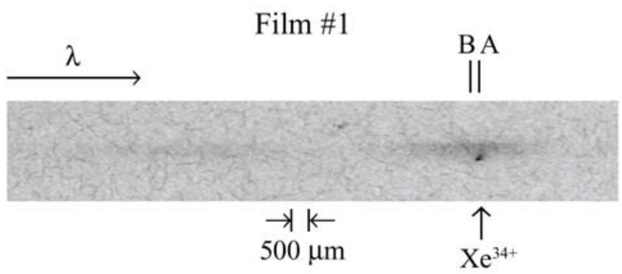

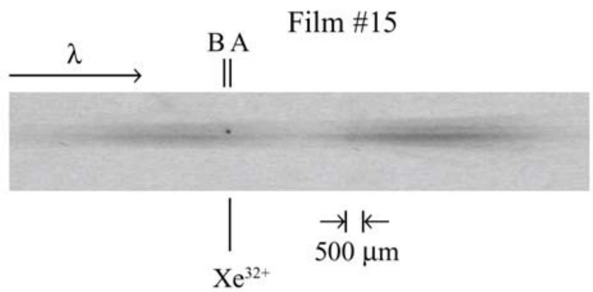

$G \sim 10^6$

$G \sim 6 \times 10^6$

J. Phys. B **36,** 3433 (2003)

From Damage (Ti foil)

$G \sim 1\text{–}5 \times 10^6$

CHANNEL STABILITY, EIGENMODE, AND CRITICAL POWER

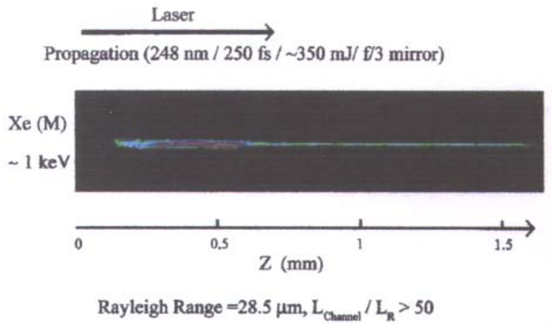

FIG. 1. Single-exposure x-ray image of a stable slender channel emitting Xe(M) radiation (≈1 keV) produced in a gaseous target containing $(Xe)_n$ clusters. The incident 248-nm pulse had a duration of ≈250 fs and an energy of ≈350 mJ, and was focused with f/3 off-axis parabolic mirror. The image was recorded with an x-ray pinhole camera having an aperture with a diameter of 25 μm and a spatial resolution of ≈30 μm. Because the Rayleigh length of the focusing system is 28.5 μm, the observed length of the channel exceeds 50 Rayleigh ranges. Additional experimental details are reported in ref. 4. The color scale (in arbitrary units) of the measured x-ray intensity is defined by black, zero; red through violet, ascending intensity; and white, maximum.

limiting the stability of the confined propagation illustrated in Fig. 1, and the evaluation of the corresponding upper bound on the power density.

Following conventional notation (1), we introduce the definitions of the coordinates of the η-ρ_0 plane given by

$$\eta = P_0/P_{cr}, \qquad \rho_0 = r_0\omega_{p,0}/c, \qquad [1]$$

with P_0 denoting the incident peak power and with the critical power (P_{cr}) given by (1, 12)

$$\boxed{\begin{aligned} P_{cr} &= (m_{e,0}^2 c^5/e^2)\int_0^\infty g_0^2(\rho)\rho d\rho(\omega/\omega_{p,0})^2 \\ &= 1.6198\times10^{10}(\omega/\omega_{p,0})^2 W, \end{aligned}} \qquad [2]$$

in which $m_{e,0}$, c, and e have their customary identifications $g_0(\rho)$ is the Townes mode (21), and ω, $\omega_{p,0}$, and r_0, are the angular frequency corresponding to the propagating radiation the angular frequency of the unperturbed plasma, and the radius of the incident intensity profile, respectively. In addition, lowest eigenmodes (1, 10, 12) exist with the dimensionless radius

$$\rho_{e,0} = \left[2\int_0^\infty U_{s,0}^2(\rho)\rho d\rho/U_{s,0}^2(0)\right]^{1/2}, \qquad [3]$$

in which $U_{s,0}(\rho)$ represents the eigenmode (1, 10, 12) with index s. The present analysis was confined to electron densities N, less than one-quarter of the critical electron density (N_{cr}) to eliminate resonant plasma wave production, and forward Raman scattering (22, 23) was not included, because it is known experimentally that it can be suppressed (24).

Fig. 2 illustrates the geography in the η-ρ_0 plane of the stable and unstable regions characteristic of channel formation in initially homogeneous plasmas (1). The essential features are the locus of the eigenmode curve $\rho_{e,0}(\eta)$ defined by Eq. **3**, the existence of a region of stable propagation that includes the

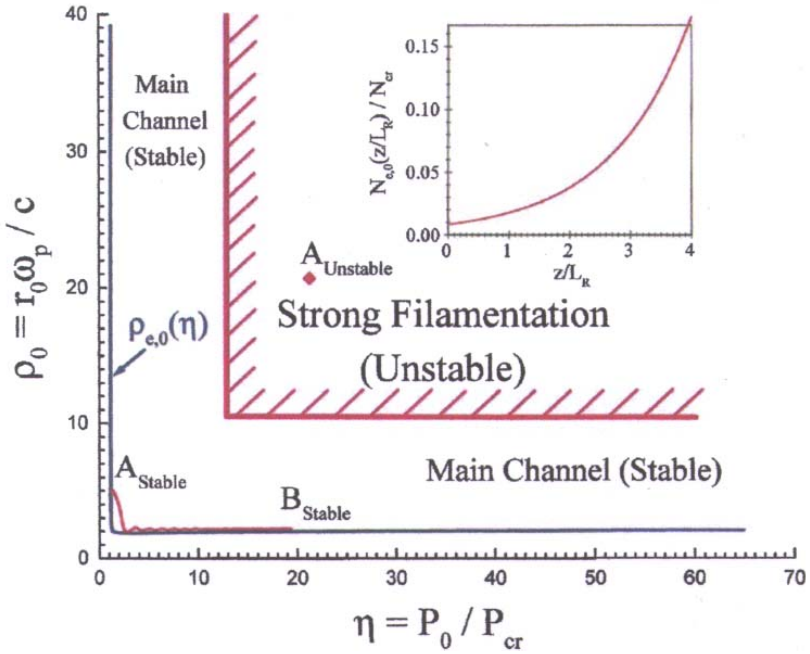

FIG. 2. Stability map in the η-ρ_0 plane for relativistic and charge-displacement self-channeling of Gaussian beams in initially homogeneous plasmas. The dimensionless coordinates ρ_0 and η are defined by Eq. **1**. Stable and unstable regions in plane (η, ρ_0) and the locus $\rho_{e,0}(\eta)$ for the lowest eigenmodes are shown. Point A_{UNSTABLE} (21.1, 20.6) corresponds to the input pulse shown in Fig. 3*A*. Points A_{STABLE} and B_{STABLE} and the trajectory connecting them are described in the text. B_{STABLE} corresponds to the intensity distribution given in Fig. 3*C*. (*Inset*) The exponential longitudinal (z) electron density profile [$N_{e,0}(z) = N_{e,0}(0)\exp(\alpha z)$, $N_{e,0}(z = 3.95\,L_R) = 20\,N_{e,0}(0) = 1/6\,N_{cr}$] between points A_{STABLE} and B_{STABLE}, and L_R denotes the Rayleigh range.

Brightness Comparison

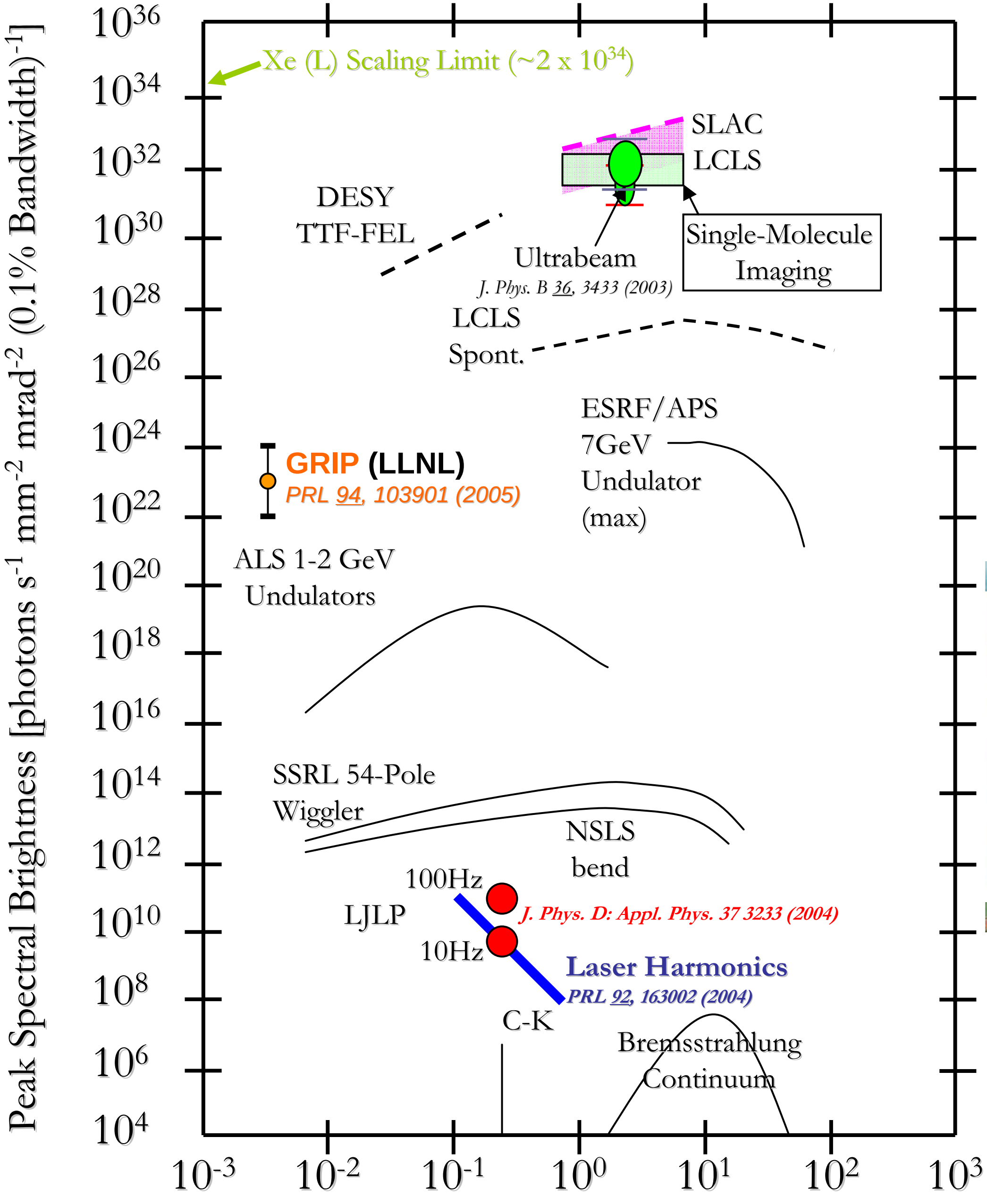

$$\frac{P}{\lambda^2} = 10^{24}–10^{25}\ \mathrm{W/cm^2}$$

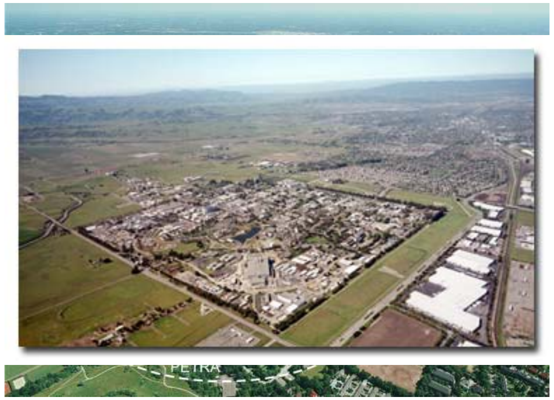

FOUR CENTURIES OF SPATIAL RESOLUTION LIMITS

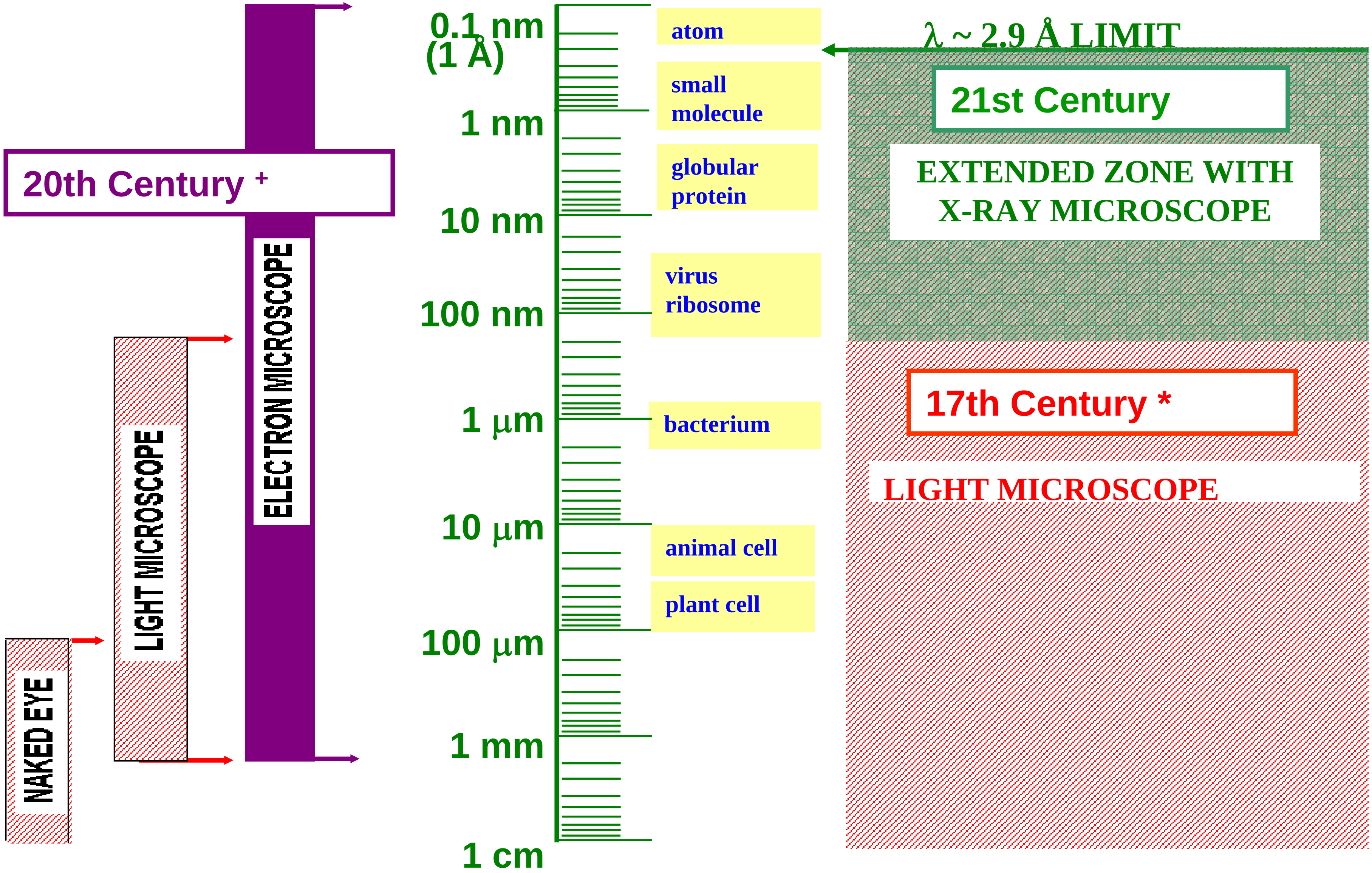

- X-RAY IMAGING EXTENDS SPATIAL RESOLUTION OF LIVING MATTER BY ~ 10^3-FOLD.

* Kepler, Hooke, Leeuwenhoek — LIVING MATTER

\+ Ruska — DEAD MATTER

Figure adapted from *Molecular Biology of the Cell*, fourth edition, edited by Bruce Alberts *et al*. (Garland Science: NY, 2002).